

Communications Research Centre

MULTI-FREQUENCY MEASUREMENT OF RADAR SEA CLUTTER AT LOW GRAZING ANGLES

by

H.C. Chan

This work was sponsored by the Department of National Defence,
Research and Development Branch under Project No. 041LC.

CAUTION

The use of this information is permitted subject
to recognition of proprietary and patent rights.

CRC REPORT NO. 1410
OTTAWA, MAY 1987

TK
5102.5
C673e
#1410



Go
De

Canada

Communications

Gouvernement du Canada
Ministère des Communications

IC

Canada

1. INTRODUCTION

2. THE RADAR FACILITY AND SITE CONDITIONS

COMMUNICATIONS RESEARCH CENTRE

2.2 Near Site Conditions

3. DATA DEPARTMENT OF COMMUNICATIONS

CANADA

3.1 Sea Clutter Data Base

3.2 Assessment of Data Quality

3.3 Signal Processing

3.3.1 Determination of the Existence of
Sea-Clutter Components

3.3.2 Suppression of Interference Components

(a) Frequency-Domain Interference Suppression

(b) Time-Domain Interference Suppression

4. ANALY MULTI-FREQUENCY MEASUREMENT OF RADAR SEA CLUTTER

AT LOW GRAZING ANGLES

by

H.C. Chan

(Radar and Communications Technology Branch)

4.2 Spatial and Temporal Correlation Analyses

4.2.1 Doppler Shift and Spectral Width of Sea

4.2.2 Sea-Clutter Spectra at Different

The use of this information is permitted subject
to recognition of proprietary and patent rights.

CAUTION

Industry Canada
Library - Queen

SEP - 4 2012

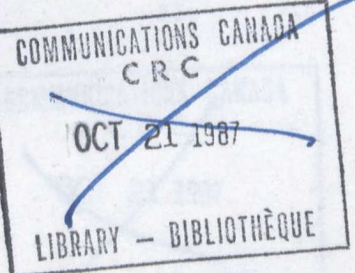
Industrie Canada
Bibliothèque - Queen

CRC REPORT NO. 1410

May 1987
OTTAWA

5. SUMMARY OF RESULTS AND RECOMMENDATIONS

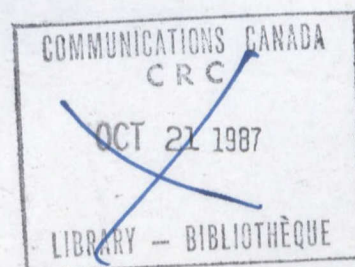
This work was sponsored by the Department of National Defence,
Research and Development Branch under Project No. 041LC.



TK
5102.5
C6732
#1410
C.b

TABLE OF CONTENTS

	<u>Page</u>	<u>No.</u>
1. INTRODUCTION	1	
2. THE RADAR FACILITY AND SITE CONDITIONS	2	
2.1 The Radar Facility	2	
2.2 Radar Site Conditions	4	
3. DATA QUALITY AND SIGNAL PROCESSING	7	
3.1 Sea Clutter Data Base	7	
3.2 Assessment of Data Quality	7	
3.3 Signal Processing	8	
3.3.1 Determination of the Existence of Sea-Clutter components	9	
3.3.2 Suppression of Interference Components	12	
(a) Frequency-Domain Interference Suppression	12	
(b) Time-Domain Interference Suppression	18	
4. ANALYSES RESULTS	21	
4.1 Estimation of Sea-Clutter Radar Cross Section Coefficients	21	
4.1.1 Antenna Gain Pattern Compensation	21	
4.1.2 Dependence of σ_0 on Wave Direction, Polarization and Wave Periods	22	
4.1.3 Comparison of Sea-Clutter σ_0 with Published Data	28	
4.2 Spectral and Temporal Correlation Analyses.	28	
4.2.1 Doppler Shift and Spectral Width of Sea Clutter	30	
4.2.2 Sea-Clutter Spectra Observed at Different Look Directions.	32	
4.2.3 Sea-Clutter Decorrelation Time	38	
4.3 Statistical Analysis	40	
4.3.1 Estimation of Clutter Model Parameters	41	
4.3.2 Chi-Square Goodness of Fit of Sea-Clutter Models	43	
5. SUMMARY OF RESULTS AND RECOMMENDATIONS	49	
5.1 Summary of Results	49	
5.2 Recommendations	53	



6. APPENDICES	55
A) Summary of Wave Data for the North Truro Experiment	55
B) Computation of Sea-Clutter Model Parameters	55
7. REFERENCES	64
8. ACKNOWLEDGEMENTS	65

MULTI-FREQUENCY MEASUREMENT OF RADAR SEA CLUTTER AT LOW GRAZING ANGLES

by

H.C. Chan

ABSTRACT

Sea-clutter has been and continues to be a major source of performance limitations for maritime surveillance radar systems. An understanding of the detailed sea-clutter behaviour is important in devising signal processing algorithms aimed at optimizing radar detection performance under sea-clutter environments.

A sea-clutter measurement experiment was conducted in July 1982 at North Truro (near Cape Cod), Massachusetts. The radar equipment employed was a multi-frequency, mobile coherent radar operated by Lincoln Laboratory of the Massachusetts Institute of Technology(MIT). Sea-clutter data were collected at X, S, L, UHF and VHF bands.

Because of interferences in the UHF and VHF bands, only X-, S- and L-band data are analyzed. Analyses have been carried out examining the sea-clutter coefficient as a function of frequency, polarization and waveform resolution. Spectral characteristics of sea-clutter in up-wind, cross-wind and down-wind conditions are compared.

1. INTRODUCTION

Sea-clutter has been and continues to be a major source of performance limitations for maritime surveillance radars. In an effort to gain some first-hand experience in the characterization of sea-clutter processes, the Department of National Defence(DND) cooperated with the MIT Lincoln Laboratory in a program designed to collect and analyze radar-clutter data. This program comprises two phases. Phase '0', which began in 1979, employed a noncoherent X-band radar. Preliminary data were collected from various Canadian sites. Data from Phase '0' were analyzed, and the results were used in the selection of sites to be visited in Phase '1'. Phase '1' employs a 5-band coherent radar for the collection of detailed clutter information.

Canadian participation in Phase '0' had been limited. However, DND intends to play a more active role in Phase 1. In a memorandum of understanding between DND and Lincoln Laboratory, an agreement was reached so that clutter data collected by Lincoln Laboratory at all Canadian and

U.S. sites will be made available to Canada. On behalf of DND, the Radar Research Laboratory(RRL) of the Communications Research Centre(CRC) will analyze selected aspects of the radar-clutter data.

A sea-clutter data-collection experiment was conducted during the three week period from July 2, 1982 to July 22, 1982, at North Truro, near Cape Cod, Massachusetts. As a result, approximately 100 high density (6250 bpi) computer tapes containing calibrated sea-clutter data of various radar operating modes were obtained.

The objective of this sea-clutter data-collection experiment is three fold. First, it is to gain some experience in the collection of radar sea-clutter data. Second, it is to study sea-clutter behaviours in the shallow grazing angle regions (between 0.5 and 3 degrees). This information is useful in assessing the signal processing performance of certain airborne radar imaging algorithms. Third, it is to acquire a better understanding of radar sea-clutter so as to develop optimal signal processing techniques to combat it.

In this report, the processing and analysis of the sea-clutter data are described. Section 2 describes the radar facility and radar site conditions during the data collection period. In section 3, the North Truro sea-clutter data base and data quality are assessed. Their limitations are discussed, and signal processing techniques used to circumvent these limitations are detailed. Section 4 presents the analysis results. Section 5 presents observations of sea-clutter behaviours based on this particular experiment. Recommendations of improvement in experimental procedures are also discussed.

2. THE RADAR FACILITY AND SITE CONDITIONS

2.1 The Radar Facility

(a) Radar Transmitter and Receiver

The radar facility used in this sea-clutter experiment is a mobile multi-frequency coherent radar owned and operated by MIT Lincoln Laboratory. Table I briefly summarizes the operational characteristics of this radar. The Lincoln Laboratory mobile radar facility, which includes the antenna tower assembly, the radar transmitter and receiver, the data collection and control systems and power generators are housed in three tractor trailers. The antenna tower can be extended in sections from fifty to one hundred feet above ground level. Television cameras are mounted on top of the tower to provide a visual record of the radar site. The antenna system is mechanically driven to provide a full 360 degrees coverage. There are two modes of operation of the antenna, (a) a scan mode and (b) a step mode. In the scan mode, the antenna is rotated at a maximum constant speed of 3 degrees/sec. In the step mode, the antenna is driven to a predetermined azimuth and stopped. Data in that particular direction are then taken.

Table I: Lincoln Laboratory Radar Operational Characteristics

	VHF	UHF	L	S	X
Nominal Frequencies(MHz)	165	430	1250	3400	9100
Azimuth Beamwidth(degrees)	13	5	3	1	1
Range resolution(metres)	15, 36 and 150				
Polarization	Vertical/Vertical Horizontal/Horizontal				
Sensitivity	S/N = 12 dB (Single pulse) σ_0 = -60 dB Range = 10 km				

The radar can operate either in a vertical-transmit/ vertical-receive mode or a horizontal-transmit/horizontal-receive mode. Polarization selection is via computer control of a remote servo-mechanism which controls the orientation of the antenna feed-horns. Signal of three pulse widths, 100 nsec, 240 nsec and 1 μ sec, corresponding to range resolutions of 15m, 36m and 150m, respectively, are available for transmission. On receive matched filters can be selected for each of the three waveform resolutions.

Pulse trains can be transmitted using a maximum pulse repetition frequency(PRF) of 4000 Hz. Two versions of sensitivity time control(STC) are available, namely, (a) r^3 law(clutter return assumed to be proportional to the cubic power of range) and (b) r^4 law. Owing to the relatively low magnitude of sea-clutter returns, STC was not employed in most North Truro experiments.

(b) Data Acquisition System.

The data collection system comprises a PDP-11/34 minicomputer, two fixed disks with 5 mega-byte capacity each, two floppy disk drives, two high density magnetic tape drives and a high-speed, solid-state random-access-memory(RAM). The amount of clutter data which can be collected in an experiment is limited by the size of the RAM and the data transfer rate of the tape drive. With particular combinations of PRF, range extent and waveform resolution, various modes of clutter data for different time durations can be obtained.

The data collection process is highly automated. The input parameters for each experiment are pre-programmed in the form of a fixed-format disk file. The computer operator simply specifies the appropriate input-parameter file, and the data-collection program module will be

executed until all the desired data have been collected. At the beginning of each experiment, the computer executes a sequence of radar system performance checks which include transmit power level, noise figure estimate, A/D converter bias readings, etc. Once the RAM is full, the data are transferred to a magnetic tape via the high density tape drive. Display equipment is available to provide on-line monitoring of system operations. Two CONRAC raster-scan monitors provide synthesized PPI and B-scope displays. An A-scope display provides the monitoring of the instantaneous signal condition.

2.2 Radar Site Conditions

During the sea-clutter experiment, the radar facility was located on a high ground within the confines of the North Truro Air Force Station near Cape Cod, Massachusetts. The location of this station is shown in Figure 1. Figure 2 shows the typical setup of this experimental radar. The antenna tower was fully extended to give an effective radar height of 254 feet above mean sea level. There are three antenna systems mounted on top of the tower. X-band has its own feed and reflector. S-band and L-band share a common reflector. Similarly UHF and VHF bands share a larger reflector.

An ENDECO 949 wave buoy was leased and anchored about 4 km offshore, at about 74 degrees east of north. This wave buoy is equipped with an FM communication transceiver which transmits the wave data back to the receiving equipment at the radar site for twenty minutes each hour. The wave data recorded during the three week period are summarized in ten parameters. They are:

- number of waves
- maximum period
- mean period
- mean height
- maximum height
- period of maximum height
- significant period
- significant height
- height variance
- r.m.s. height

These data are summarized in Appendix A and are used for correlating the analysis results with the sea conditions. In addition, measuring equipment was installed near the radar site in order to monitor and record the wind direction and velocity.

The sea state estimated from the wave-buoy data was between sea states 1 and 2. Wind velocity varied between 1 mph and a maximum of 17 mph. Wind direction measured near the radar was mainly from the southwest (220 degrees to 270 degrees measured clockwise from north). It should be emphasized that the wind velocity and direction measurements were taken at the radar and not at the area illuminated by the radar.

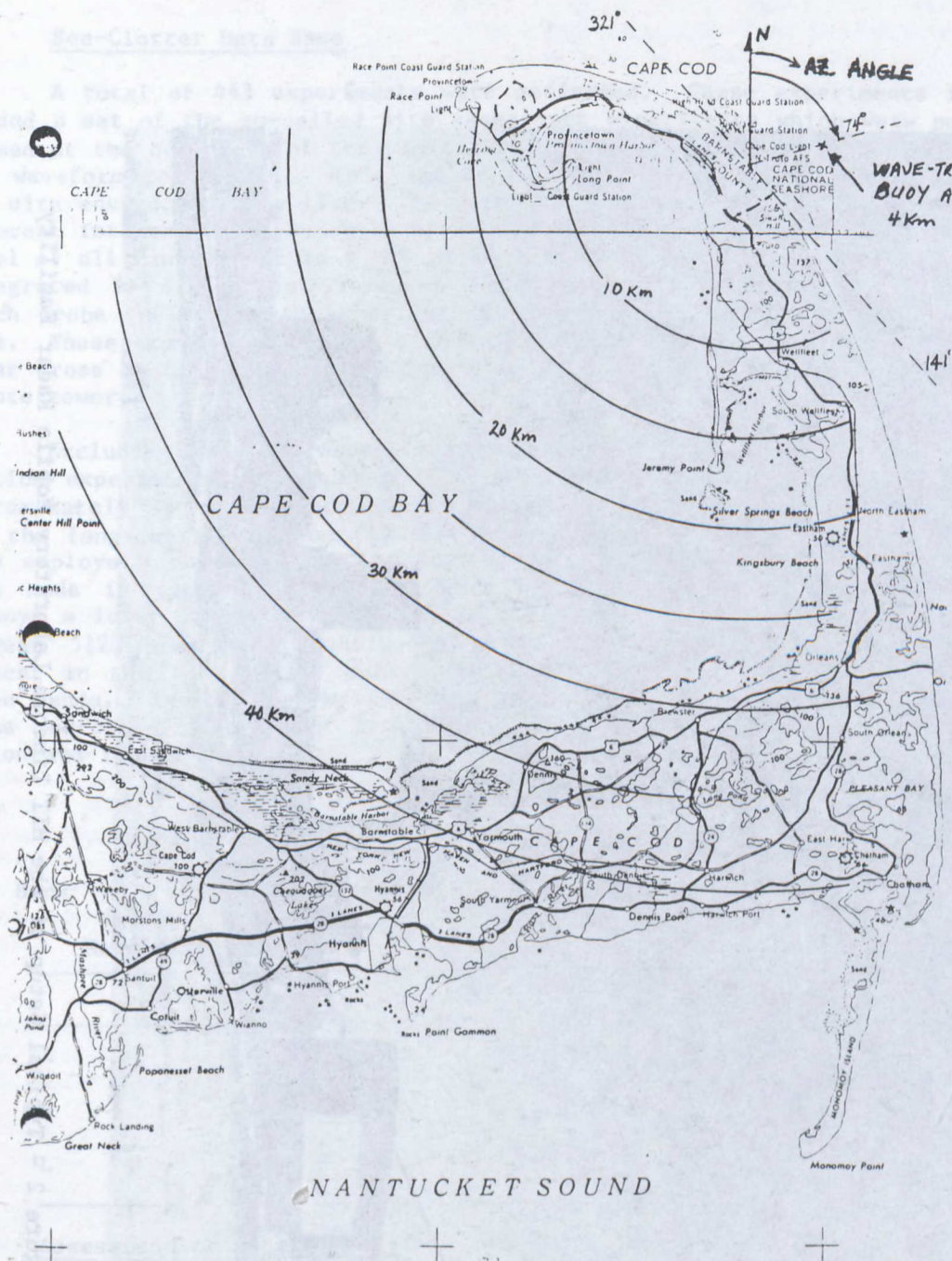


Figure 1 - Location of the North Truro Site

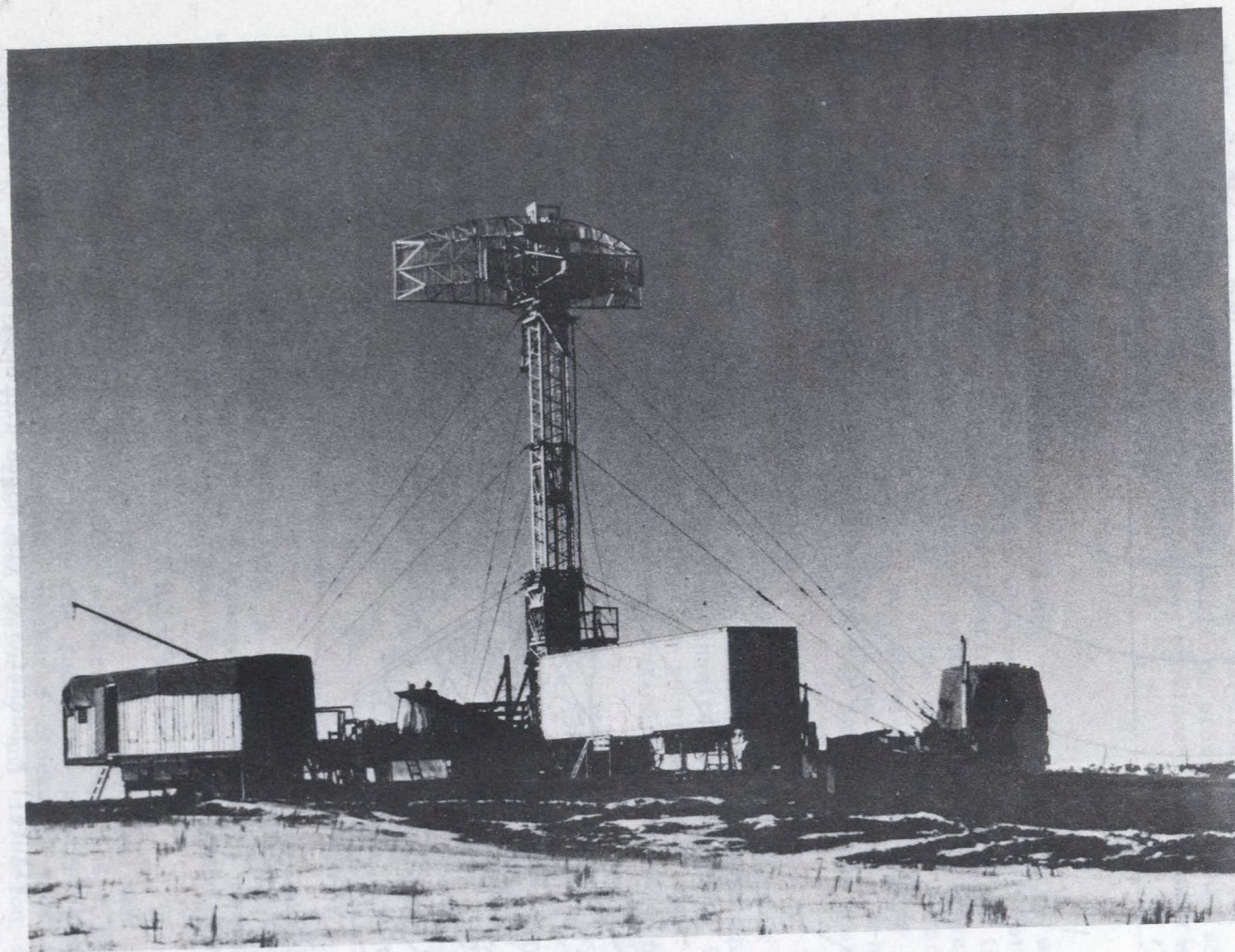


Figure 2 - Typical Setup of the MIT Lincoln Laboratory Mobile Radar Facility

3. DATA QUALITY AND SIGNAL PROCESSING

3.1 Sea-Clutter Data Base

A total of 443 experiments were performed. These experiments included a set of the so-called site assessment experiments which were performed at the beginning of the visit for each frequency band, polarization and waveform resolution. This set of data provides a good idea of what the site environment was like. The site assessment data mode employs non-coherent integration of radar returns to obtain an estimate of the clutter level of all range cells in a 360 degree scan. The usual number of pulses integrated is 128. Also included is a set of propagation experiments which probe the multipath behaviour of the radar returns near the radar site. These experiments are used to calibrate the system by measuring the radar cross section(RCS) of a corner reflector of known RCS mounted on a remote tower.

Excluding the site assessment experiments and the multi-path calibration experiments, the number of experiments suitable for analysis is approximately 350. The data may be divided into two categories, namely, (a) the long-dwell mode and (b) the short-dwell mode. The short dwell mode employs a moderate PRF, typically 4000 Hz. Data record length for this mode is typically 1024 contiguous pulses. The long dwell mode employs a lower PRF, typically 500 Hz. This mode has long data records, between 5120 and 10000 contiguous pulses. Because of interferences present in the VHF and UHF data, the analyses are confined to the upper three bands. Table II shows the breakdown of X-, S- and L-band experiments performed in terms of frequency band, polarization, waveform resolution and length of dwell.

Table II: X-, S- and L-Band Experiment Breakdown

Band	H-Polarization				V-Polarization				
	Waveform	15m		150m		15m		150m	
	Resolution								
	PRF	4000	500	4000	500	4000	500	4000	500
X		7	6	9	6	10	6	12	33
S		10	4	14	9	14	8	15	32
L		6	3	11	3	9	3	12	21

3.2 Assessment of Data Quality

There are three main sources of interference in the sea-clutter data, namely, ground clutter received from the antenna sidelobes, receiver

noise and interference from local communications channels. Published data in the literature[1]-[7] indicate that the radar cross section coefficients(σ_0) of sea clutter, defined as the effective radar cross section(σ) per unit area, at microwave frequencies are below -30 dB at almost all sea states for shallow grazing angles (0 to 10 degrees). Ground clutter, on the other hand, has an extremely wide dynamic range, which spans several decades of dBs. The sidelobe levels of the radar antenna are not exceptionally low. Consequently, it is possible that the ground returns from the antenna sidelobes may actually have a significantly higher magnitude than the sea-clutter component received from the antenna mainlobe.

Radar receiver noise is also a source of interference which could produce erroneous sea-clutter measurements if left untreated. The raw sea-clutter data are calibrated in Lincoln Laboratory. Calibration refers to the process of translating the digitized coherent sea-clutter samples taken from each range cell into an instantaneous value of equivalent radar cross section. Since the calibration of radar clutter is based on the radar equation, it assumes an inverse fourth power dependence of clutter power with range. The receiver noise, on the other hand, is independent of range. Consequently, after calibration, the noise component is effectively multiplied by a constant proportional to the fourth power of the range.

Interference from local communications channels is another source of error in the sea-clutter data analysis. This kind of interference occurred mainly at L-band, UHF and VHF frequencies. There is an L-band radar located at the North Truro Air Force Station, which is not far from the Lincoln Laboratory facility. This radar was continuously in operation during most of the experimental period. The interference at L-band did not present too much of a problem in the analysis because it can be readily identified. Interference at UHF and VHF bands proved to be the most serious. This interference, which behaved much like jamming signals, might have come from local television channels. Figure 3 shows a PPI display derived from data of a VHF experiment. High returns from random directions are evident. Interference at UHF was observed to be most serious, as a result, UHF data collection was discontinued after initial assessment of the data.

Occasionally, there was interference from moving objects such as aircraft, boats, birds and automobiles. However, this occurred in isolated range cells and can be readily identified. Rain clutter was also present in some experiments.

3.3 Signal Processing

Since the sea-clutter data may contain ground clutter, receiver noise and interference components, it is essential that they be removed or at least suppressed so as not to obscure the result of the analyses. In this section, some of the signal processing techniques used in the identification and suppression of unwanted signal components are described.

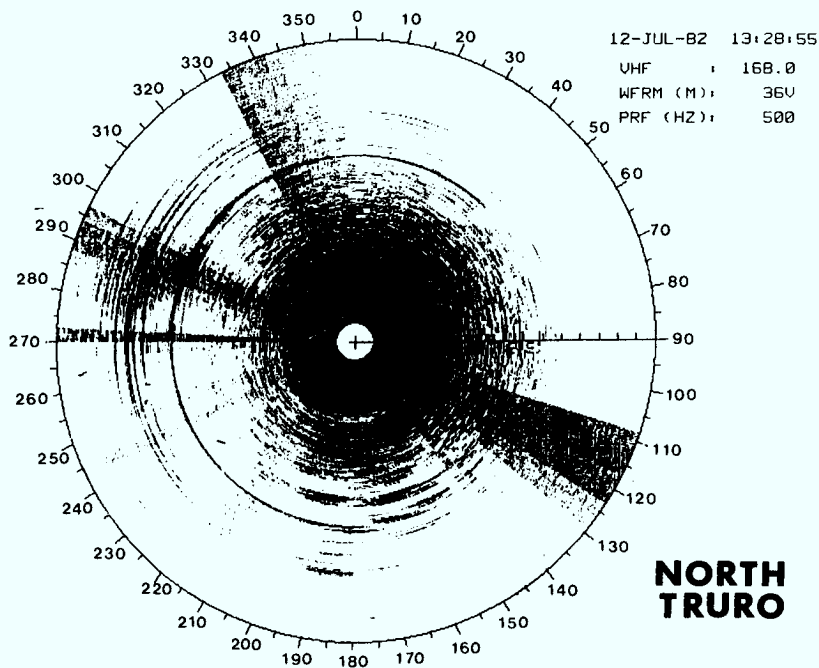


Figure 3 - PPI Display from VHF Data

The first step in the analysis of sea-clutter data is the determination of the existence of sea-clutter components in the recorded data. The next step is to remove or suppress unwanted signal components. Finally, analyses are performed on the resulting data which should contain mainly of sea-clutter components.

3.3.1 Determination of the existence of sea-clutter components

In order to determine whether sufficient amount of sea-clutter components are present in the recorded data, both time-domain and frequency-domain analyses are employed. For each experiment, the data are scanned by a computer program which produces two sets of results. The first is a plot of the effective σ vs range for the sea-clutter data. The radar cross section, σ , of the sea-clutter at each range cell is computed as the mean squared value of the data samples. In subsequent discussions, the term " σ vs. range profile" will be used to refer to the result of the above computation. The σ vs. range profile for each experiment was computed and stored as disk files. They can be accessed by special display software in order to determine visually the presence of sea clutter components in a particular experiment. A typical σ vs range plot is shown in Figure 4. Trace A is derived from a data set containing a strong sea-clutter component. The presence of sea-clutter component is clearly visible from

2 km out to about 7 km. Trace B is derived from a data set which contains almost no sea-clutter component. The dependence of the magnitudes of these data, composed mainly of receiver noise component, on the fourth power of range is evident. This r^4 dependence is introduced by the calibration process. The σ vs range plot is useful in identifying the usable range of sea-clutter data. For example, for the experiment corresponding to Trace A of Figure 4, the analysis would be restricted to data corresponding to ranges less than 6 Km. Trace B of Figure 4 represents the noise floor for experiments having identical parameters such as frequency, polarization and waveform resolution. We shall consider data within a certain range interval as usable sea-clutter data if the majority of the range cells within that interval have a σ value at least a number of dB (typically 5 dB) higher than the noise floor. Data which do not meet the above criterion will not be analyzed.

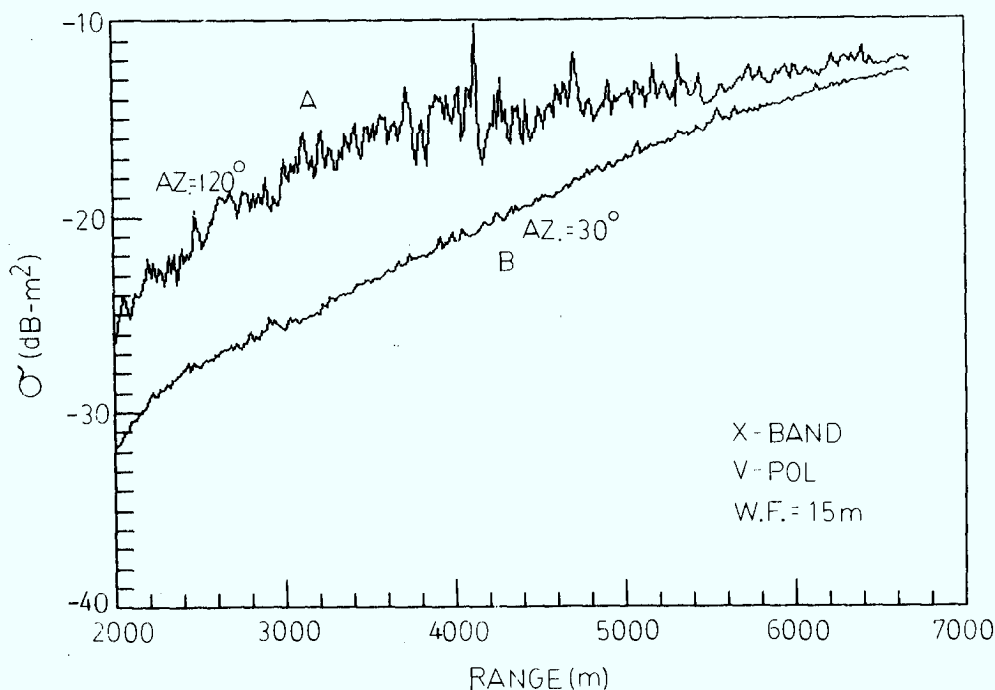


Figure 4 - Typical σ vs Range Plot of Sea Clutter

The second set of results produced by the data scanning computer program is the typical sea-clutter spectra of the data. In order to identify the presence of ground clutter and other interferences, spectral analysis is performed using the method of averaged periodograms[8]. Several range cells in each dwell of an experiment are selected for spectral analysis. These range cells are typically at close ranges ($R < 5$ km from the radar), at which sea-clutter components are expected to be

present. The radar returns for these range cells are collected into separate data records. The entire data record is segmented into a number of equal-length sub-sequences, typically 1024 complex samples. Each sub-sequence is multiplied by a Hamming[9] data window and then fast Fourier transformed(FFT). The FFTs of all the sub-sequences are averaged. The squared magnitude of the averaged FFTs is called the periodogram which represents the power spectrum of the sea-clutter for that particular range. Figure 5 shows the power spectrum of the data for an X-band experiment. This result shows a well-defined sea-clutter spectral component. The large spectral line at zero Doppler frequency is the ground-clutter component received from the antenna sidelobes. It can be seen that the ground-clutter actually has more power than the sea-clutter component.

The use of spectral analysis and the σ vs. range profile plot to identify various signal components in the data works very well. Occasionally, there are other anomalies in the data. They can usually be resolved by examining the coherent clutter samples themselves. For low-frequency bands (L-band or lower), the Doppler shift of the sea-clutter component is relatively small for typical water wave movements. Consequently, the sea-clutter spectrum cannot easily be separated from ground clutter.

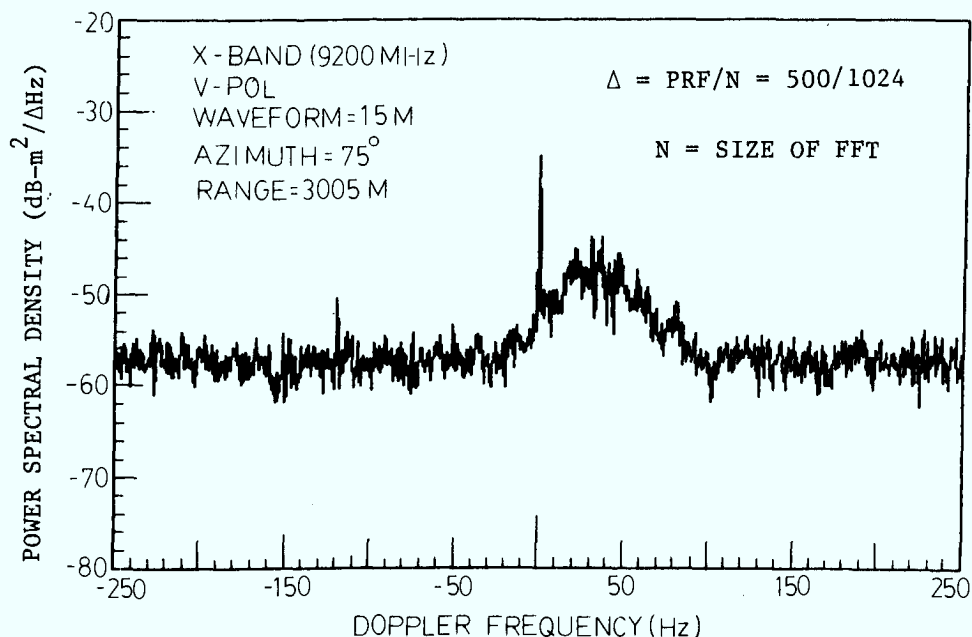


Figure 5 - Typical Power Spectrum of X-band Sea Clutter

Figure 6a shows the σ vs range plot of an L-band, horizontal polarization experiment. The return from the range cell corresponding to a range of 1.3 km has a significantly higher magnitude than those of the other range cells. The I-channel waveform of the data from this range cell is shown in Figure 6b for a duration of 2560 samples. The PRF was 4000 Hz. It resembles a saturated sinusoidal wave with a period of approximately 0.5 second. This corresponds to a Doppler shift of 2 Hz which, at L-band, translates to a radial velocity of about .5 mph. In contrast, the I-channel waveform of the data from a range cell corresponding to 1.0 km is shown in Figure 6c. This waveform is composed mostly of low-frequency random noise components and is most likely a result of sea-clutter. The waveform for the range cell at 1.0 km is typical of most range cells in the same direction. Consequently, it can be assumed that something besides sea-clutter is responsible for the peculiar waveform observed in the range cell at 1.3 km. One can only speculate what the cause of this saturated sinusoidal behaviour from radar returns might be. One plausible scenario is that the data in Figure 6b are actually returns from a fairly large boat travelling in a direction almost perpendicular to the radar look direction. The saturation is probably caused by the omission of an attenuator in the receiver chain, in anticipation of the low magnitude of sea echoes. In any case, the existence of sea-clutter components in the data can be determined quite accurately by using one or more of the above methods.

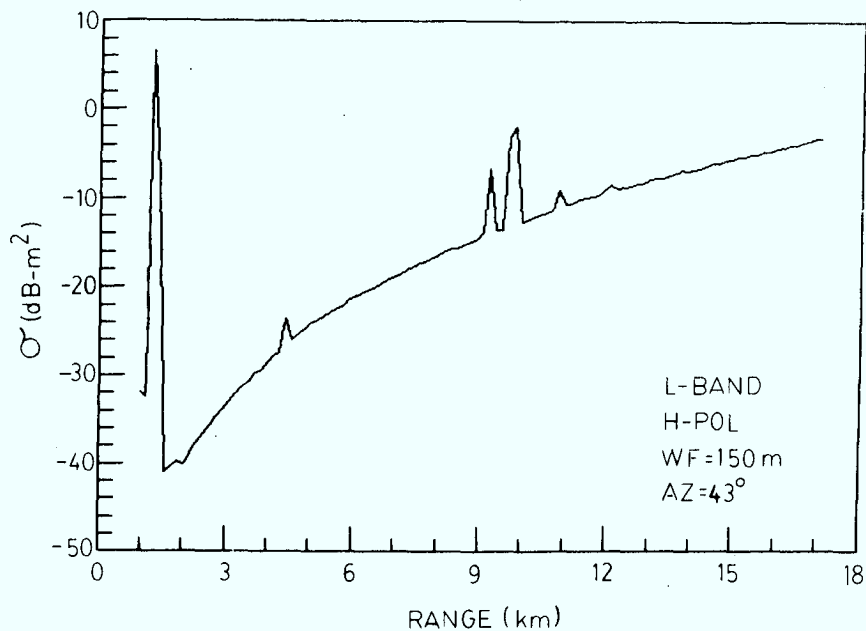
3.3.2 Suppression of Interference Components

Since ground clutter is mostly the result of radar returns from stationary objects, there will be very little Doppler shift in ground-clutter spectral components. However, for very strong ground clutter, the leakage[8] caused by the FFT may spill over to neighbouring Doppler bins. This effect is suppressed to some extent by employing the Hamming window. In order to obtain a reasonably accurate estimate of the σ_0 of the sea-clutter and to perform statistical analysis, data containing mainly of sea-clutter components must be obtained. This requires not only the removal of the ground-clutter components, but also the suppression of receiver noise components. Most of the ground-clutter and receiver noise components may be removed from the data either in time domain or in frequency domain.

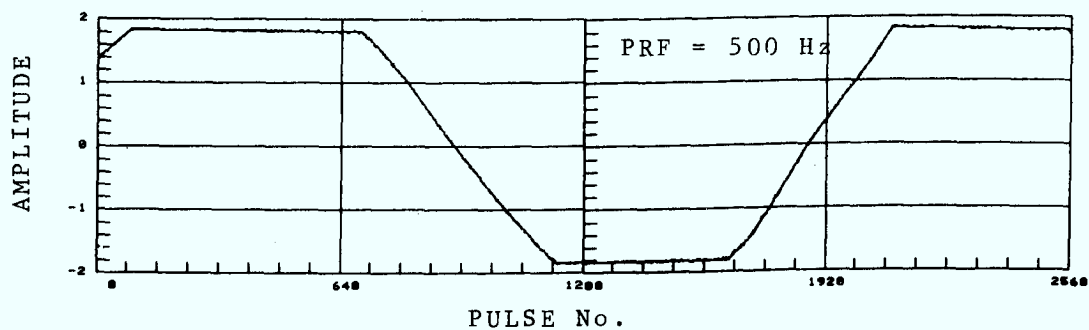
(a) Frequency-Domain Interference Suppression.

For the purpose of determining the σ_0 of sea-clutter, the frequency domain approach is employed. To suppress the ground clutter component, the values of the three Doppler-bins of a sea-clutter spectrum centred about zero Doppler frequency are replaced by the averaged values of their immediate neighbouring Doppler-bins.

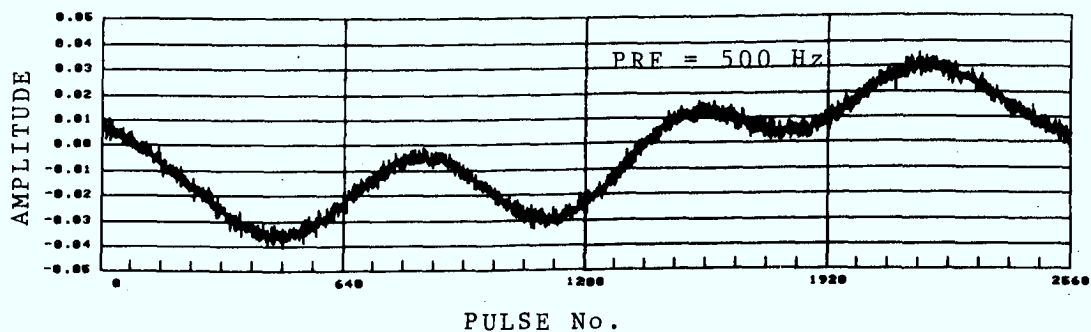
In most cases, ground clutter is comprised of a relatively large component at zero Doppler and a weaker component with some degree of spectral spread. The large zero-Doppler component is a result of returns from



(a) σ vs. Range Profile of an L-band, H-Pol Experiment



(b) I-channel Waveform of Returns From 1.3 km.



(c) I-channel Waveform of Returns From 1.0 km.

Figure 6 - Anomalies in L-band, Horizontal Polarization
Sea-clutter Data

stationary objects such as the ground, buildings and tree-trunks, etc. The weaker component is a result of returns from movable objects such as leaves and vegetations. It is the large zero-Doppler component which could contribute significant ground-clutter energy from the antenna side-lobes. Let the spectral component of the averaged periodogram computed from the data be $\{F_1, F_2, \dots, F_N\}$. The three Doppler bins in which most ground clutter components might be found are F_1, F_2 and F_N , representing Doppler frequencies $f_d=0$, $f_d=PRF/N$ and $f_d=-PRF/N$ respectively, where N is the size of the FFT. The ground-clutter component is suppressed by performing the operations defined below:

$$\begin{aligned} F'_1 &= \frac{F_2 + F_{N-1}}{2} \\ F'_2 &= \frac{F_3 + F_4}{2} \\ F'_N &= \frac{F_{N-2} + F_{N-3}}{2} \end{aligned} \tag{1}$$

This procedure is valid if either or both of the following conditions are satisfied:

- i) The sea-clutter spectrum has a reasonably broad Doppler spectral width, and the spectral rolloff of the sea clutter is relatively gradual around zero Doppler.

Or,

- ii) The sea-clutter spectrum is completely shifted away from zero Doppler. In this case, the spectral component around zero would comprise only ground clutter and receiver noise components. Since receiver noise has a flat spectrum, it is expected that the spectral value of the receiver noise at zero Doppler would be very close to that of its neighbouring Doppler bins.

Figure 7 shows the resulting spectrum after the operation defined in Eqn(1) has been carried out on data whose spectrum is shown in Figure 5. It can be seen that the ground clutter spectral line at zero Doppler frequency has been effectively removed and the sea-clutter spectrum remains almost unchanged.

The effective radar cross section of sea-clutter may be obtained by integrating the sea-clutter power spectrum (power spectral density). Receiver noise component suppression is accomplished by restricting the

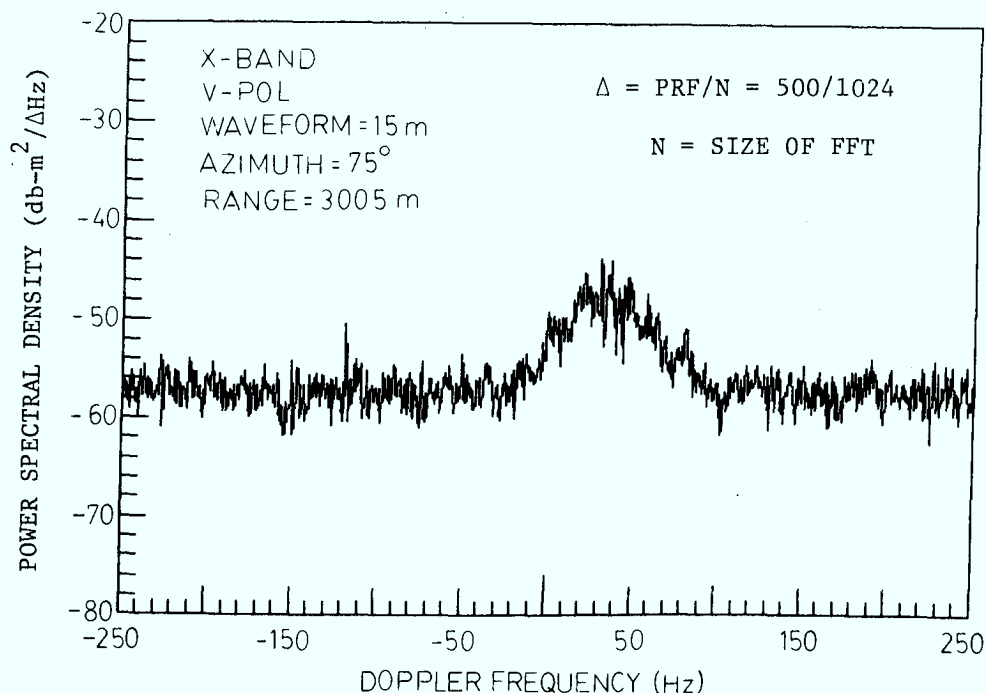


Figure 7 - Sea-Clutter Power Spectrum after Suppression of Ground Echo

integration limits of the sea-clutter spectrum to values which encompass the bulk of the visible clutter spectrum. The averaged periodogram for each range cell is computed from the sea-clutter samples, and an estimate of the proper integration limits is obtained by a visual inspection of a representative sea-clutter spectra for the particular experiment. The accuracy of this estimate depends on the sea-clutter spectrum rolloff. If the sea-clutter spectrum has a long spectral tail, then there is a trade-off between cutting off some of the sea-clutter power and including some receiver noise power in the estimate. It is of interest to obtain some idea of the magnitude of the error in the estimate of σ_0 introduced by the receiver noise component.

Consider a Gaussian shaped sea-clutter spectrum centred at zero-Doppler frequency:

$$P(f) = \exp\left\{-\frac{f^2}{k\sigma_f^2}\right\}$$

where

$$\begin{aligned}
 \sigma_f &= 0.5 \times (3\text{dB spectral width}) \\
 k &= 1.44 \text{ so that when } f = \sigma_f, P(f) = 0.5 \\
 -\frac{W}{2} &\leq f \leq \frac{W}{2} \quad (W = \text{Doppler bandwidth})
 \end{aligned} \tag{2}$$

It is assumed that the Doppler bandwidth W is at least several times greater than σ_f , so that sea-clutter energy at the edges of the Doppler band is negligible. Since we are dealing with sampled data, a discrete version of Eqn(2) will be considered. Except for a proportional constant depending on the sampling rate of the spectrum, the discrete spectrum will have a similar shape as that described by Eqn(2):

$$P(n\Delta f) = \exp\left\{-\frac{(n\Delta f)^2}{k\sigma_f^2}\right\} \tag{3}$$

$$n = -\frac{N}{2}, -\frac{N}{2}+1, -2, -1, 0, 1, 2, \dots, \frac{N}{2}$$

where

Δf is the resolution of the discrete Gaussian spectrum.

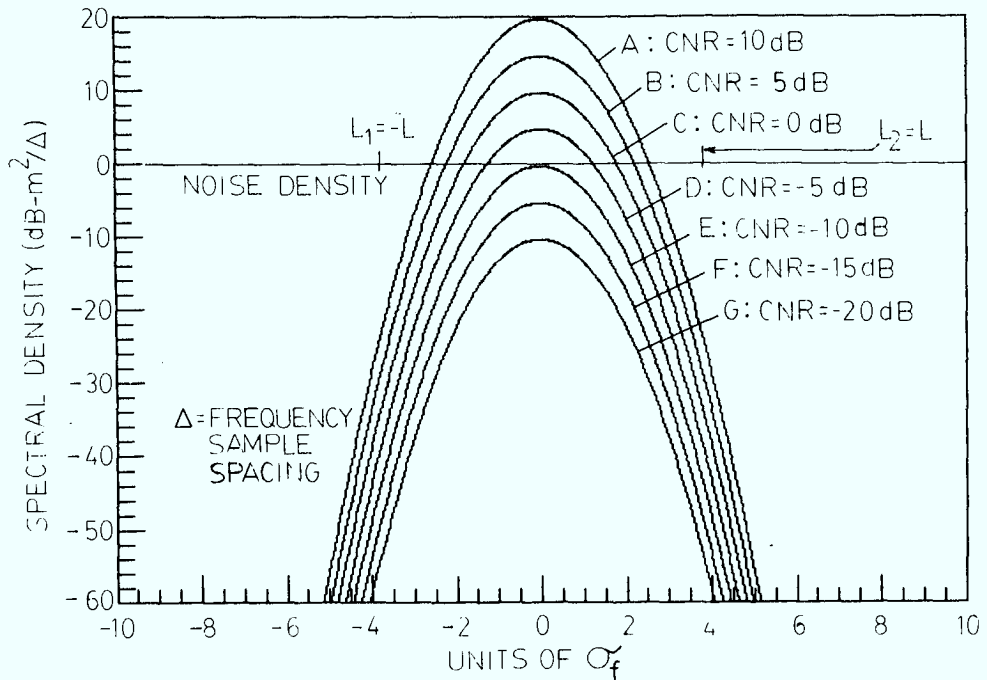


Figure 8 - Sea-clutter Power Estimation by Integration of Power Spectral Density

In the absence of receiver noise, the total clutter power can be estimated by integrating the Gaussian function over the Doppler bandwidth. Figure 8 shows the Gaussian-shape spectra for several values of clutter-to-noise ratio. For example, in Trace A, the summation under the Gaussian curve over the Doppler bandwidth is 10 dB greater than the summation of the noise density (0 dB line). We shall denote the sea-clutter power by C:

$$C = \sum_{n=0}^{N-1} P(n\Delta f) \quad (4)$$

where N is the number of spectral samples representing the sea-clutter spectrum over the Doppler bandwidth

Let N_0 be the discrete power density of the receiver noise, so that the noise power within the Doppler band is $N_0 N$. An estimate of the sea-clutter power may be obtained by integrating the estimated sea-clutter spectrum over a limit less than or equal to the Doppler bandwidth. This estimate is given in Eqn(5):

$$C' = \sum_{n=L_1}^{L_2} P(n\Delta f) + N_0(L_2 - L_1) \quad (5)$$

The clutter-to-noise ratio can be defined as:

$$CNR = \frac{C}{N_0 N} \quad (6)$$

For a given value of CNR, the sea-clutter power estimated from the mean-squared value of the sea-clutter samples will contain a certain amount of error due to the noise component. Let us define a parameter δ to represent the percentage error of the sea-clutter power estimate as:

$$\delta = (C' - C)/C \times 100\% \quad (7)$$

This error will be a function of the integration limits. Referring to Figure 8, the lower and upper integration limits are designated as $L_1 = -L$ and $L_2 = L$, respectively. Figure 9 shows the estimation-error of sea-clutter power, in terms of percentage of the actual value, as a function of integration limit(L), for several values of CNR. The integration limits are expressed in terms of units of σ_f , the standard deviation of the Gaussian spectrum. It can be seen that, for high CNR (above 5 dB), the selection of the integration limit is not very critical. For low CNR values, however, significant error will result if the integration limits are not selected properly. Consequently, data with very weak sea-clutter components will not be analyzed.

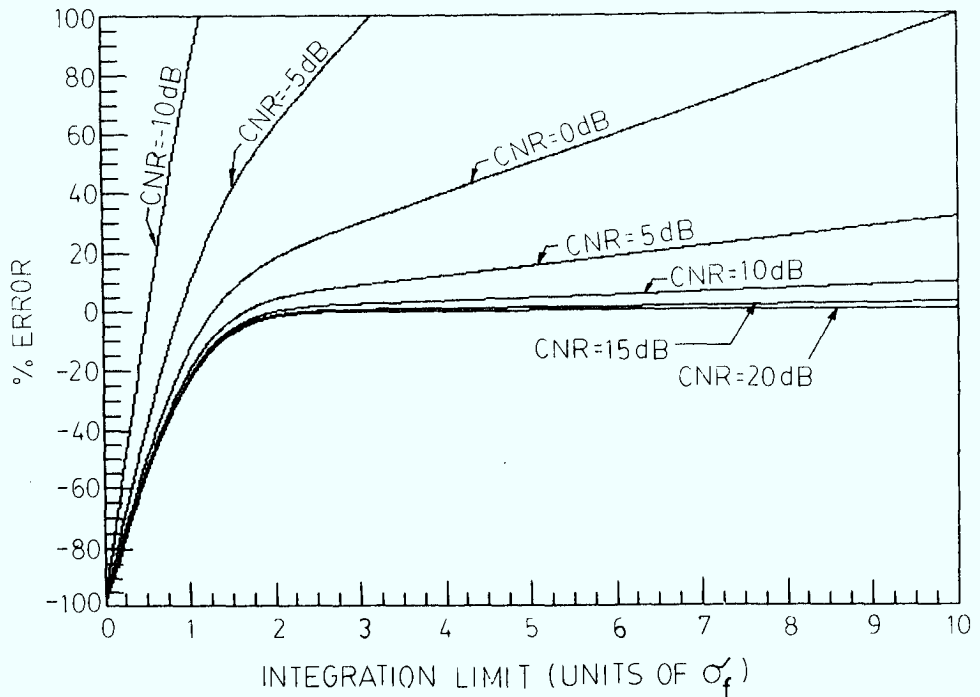


Figure 9 - Percentage Error of Sea Clutter Power Estimate as a Function of Integration Limits

Figure 10 compares the sea-clutter power estimate of a data set between two cases: (a) sea-clutter power estimate with interference suppression and (b) sea-clutter power estimate without interference suppression. This result is obtained from an S-band, horizontal polarization experiment. The waveform used was 15 m. Trace A of Figure 10 represents the sea-clutter power estimate computed from the mean-squared values of the data from each range cell. This result includes both ground-clutter component as well as receiver noise. From the typical spectrum of this data set, the sea-clutter spectrum is found to concentrate within the frequency limits of -5 Hz and 75 Hz. After the ground-clutter component is removed, the periodogram is then summed over the limits from -10 Hz to 80 Hz. The resulting sea-clutter power as a function of range samples is shown in Trace B. It can be seen that significant amount of error in the σ estimate is reduced. The value of σ_0 is obtained by dividing σ with the patch area corresponding to that range.

(b) Time-Domain Interference Suppression.

For the purpose of performing statistical analyses, time domain samples of sea-clutter with interference components are required. This is accomplished by employing digital filters. Either recursive or non-

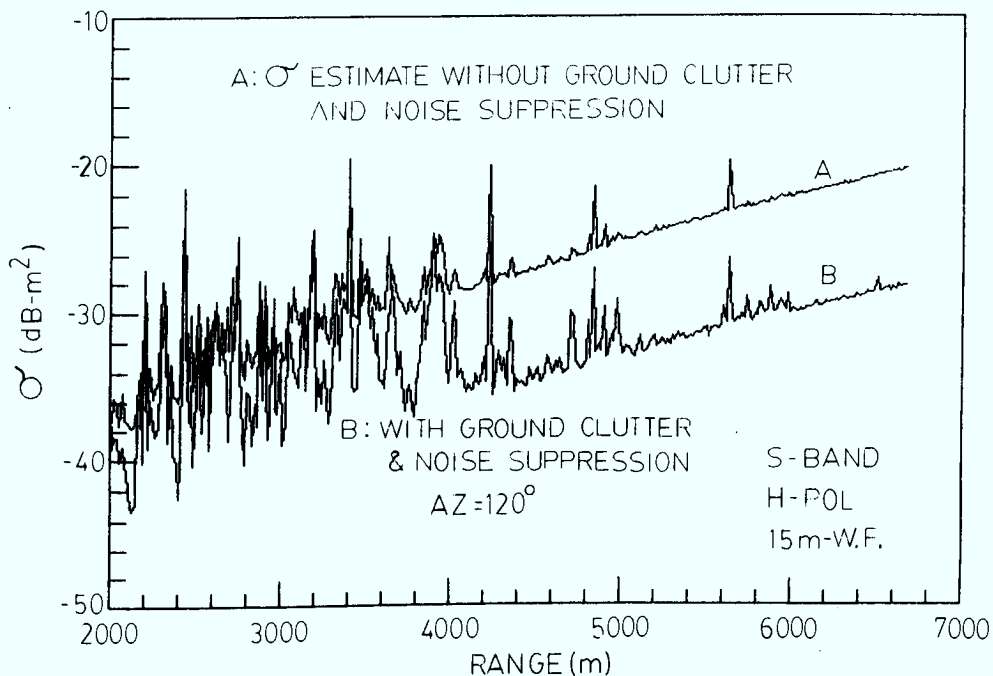
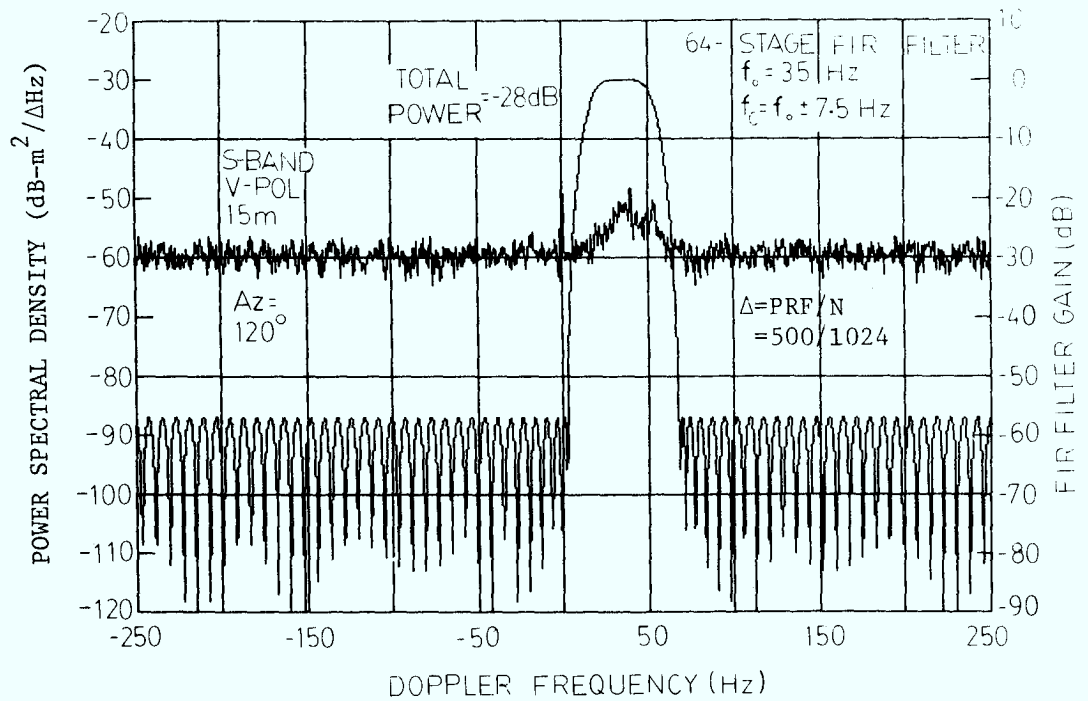


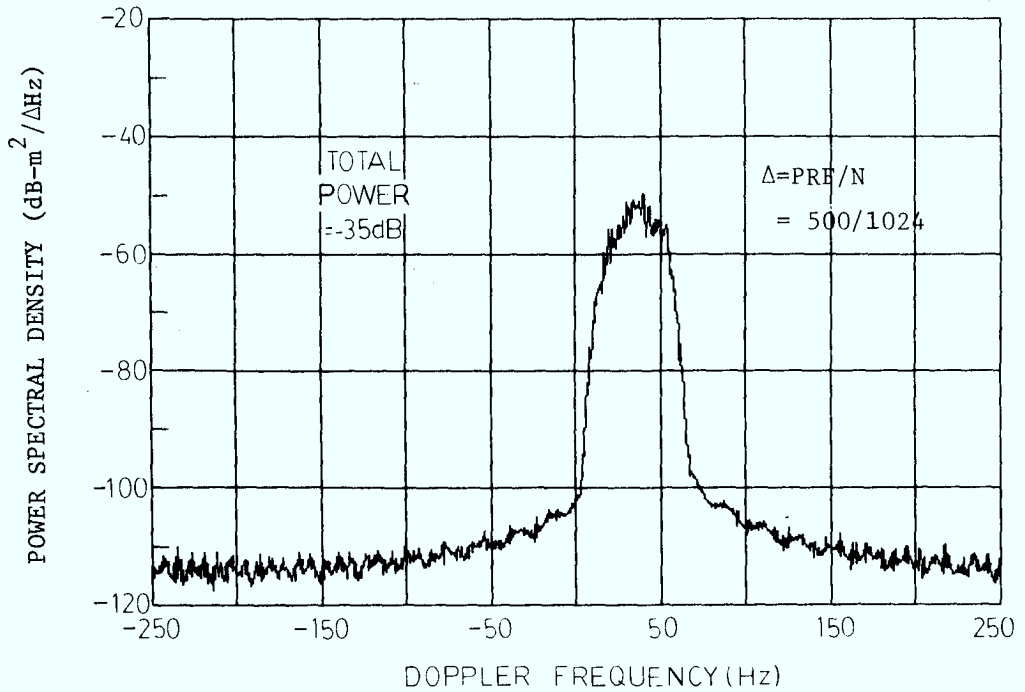
Figure 10 - Comparison of Sea-Clutter Power Estimate Between Cases with and without Interference Suppression

recursive filters may be used. Filtering may be performed either in time domain or in frequency domain. In our analysis, the time domain approach was employed. Prior to performing statistical analysis, the ground clutter component is removed from the data, and the resulting samples are filtered by an appropriate non-recursive digital filter having a passband which matches that of the sea-clutter spectrum.

In Figure 11a the periodogram of a data set obtained from an S-band, horizontal polarization experiment at a range of 4000 m. was shown. Ground clutter pick-up from antenna sidelobes can be identified as the spectral line at zero-Doppler. Superimposed on the figure is the frequency response of a 64-stage Butterworth FIR filter with a centre frequency of 35 Hz and ± 7.5 Hz passband. This filter was used to extract the sea-clutter component. Figure 11b shows the resulting sea-clutter spectrum after ground clutter removal and filtering. The estimated values of σ before and after interference suppression are -28 dB and -35 dB respectively.



(a) S-band sea-clutter spectrum and FIR filter response.



(b) Filtered sea-clutter spectrum.

Figure 11 - Time Domain Interference Suppression of Sea Clutter Data

4. ANALYSIS RESULTS

Most of the experiments were designed to examine the sea-clutter characteristics in different azimuths (look directions) within a short time span, so that sea conditions would be virtually identical. These look directions are arbitrarily separated by an angular distance of 45 degrees. Assuming that the wind direction and velocity do not change during the period of data collection, conditions approximating to the up-wind and down-wind conditions can be obtained. Because of the location of the radar, it was not always possible to collect sea-clutter data from the exact up-wind and down-wind conditions. Furthermore, it was found from the analyses of the data that the wind direction measured at the radar site did not always coincide with the water-wave direction. Water waves travelling towards the shore at a certain direction would be reflected toward a different direction. Consequently, in subsequent discussions, the terms up-wind and down-wind will be used to describe the cases, where the sea-clutter data exhibit positive and negative Doppler shifts in their spectra, respectively.

4.1 Estimation of Sea-Clutter Radar Cross Section Coefficients

The most widely used parameter in the study of radar-clutter processes is the clutter coefficient σ_0 . The clutter coefficient is defined as the effective radar cross section per unit area:

$$\sigma_0 = \sigma/A \quad (8)$$

where σ = effective radar cross section of
the sea-clutter from a range cell.

and A = patch area of the range cell
= $R\theta (cT/2) \sec\phi$

where R = range
 c = speed of light
 T = pulse length
 θ = 3 dB azimuthal antenna beamwidth
 ϕ = grazing angle.

The magnitude of σ_0 is a function of many physical parameters such as wind speed, wind direction, wave height, wave period, sea state, etc. Unfortunately, these parameters are not independent of one another, and attempts to treat σ_0 as a simplistic function of a single parameter such as sea state may produce misleading results.

4.1.1 Antenna Gain Pattern Compensation

The wavefront of a transmitted radar pulse strikes the sea surface in each range cell at varying grazing angles. At long ranges, the grazing angle approaches zero and begins to increase with decreasing range. Consequently, the returns from all the range cells in a fixed look direction

may be used to compute σ_0 as a function of grazing angle. This may be regarded as taking a single snap-shot of the σ_0 of the sea-clutter at the time of a particular experiment. Figures 12 and 13 show the elevation pattern of the S-band and X-band antennas, respectively, measured at a typical frequency within the respective radar band. It can be seen that the gain drops off quite rapidly as the angle increases beyond 4 degrees. Figure 14 plots the grazing angle as a function of range for a radar height of 254 feet assuming a flat-earth. The values of the grazing angle ranges from close to 0 at large ranges to 4.4 degrees at a minimum range of 1 km. For S- and X-band, which have relatively narrow elevation beam-widths, the sea-clutter return decreases rapidly at close ranges because of the roll-off of the elevation antenna gain. During data calibration, the gain of the antenna was used. This gain, however, refers to the value at zero degree elevation. In calculating σ_0 of the sea-clutter for X- and S-bands, the antenna elevation pattern is used to compensate for this loss of signal.

4.1.2 Dependence of σ_0 on Wave Direction, Polarization and Wave Periods

In this section, the dependence of σ_0 of sea-clutter on polarization, wave direction and wave period will be highlighted. The radar cross section coefficients of the sea clutter data are calculated for each range cell in a region which has been determined to contain sea-clutter components. The effective radar cross section area of the clutter at each range cell is computed via frequency domain integration of the sea-clutter power spectrum over the limits which the observable sea-clutter spectrum spans. The σ_0 values are then obtained by dividing the result by the corresponding patch area and applying elevation gain compensation.

In Figure 15, plots are given of values of σ_0 vs grazing angle for typical X-band experiments. In this experiment, data were taken in three look directions. This plot compares the value of σ_0 for X-band data as a function of grazing angle in different look directions. The averaged Doppler shifts of the data taken for a vertical polarization experiment at azimuths 120°, 75° and 30° are +60 Hz, +30 Hz and -30 Hz respectively. For the sake of clarity, only the results corresponding to 120° and 30° azimuths are shown. The data recorded in these two azimuthal directions correspond, approximately, to the up-wind and down-wind conditions, respectively. The estimated value of σ_0 is substantially higher in the 120° azimuth than those in the 30° azimuth. Although these look directions might not have represented the exact up-wind and down-wind directions, the ratio of the σ_0 values measured in these two direction should give a first order estimate of the upwind-to-downwind ratio of σ_0 . As much as 10 dB difference was observed.

Superimposed on the figure are the results for a horizontal polarization experiment performed within five minutes of that of the vertical polarization experiment. Thus, the sea surface conditions were very similar for the two cases. There is little difference in the magnitude of

S-BAND: 3.2 GHZ POL: HORIZONTAL

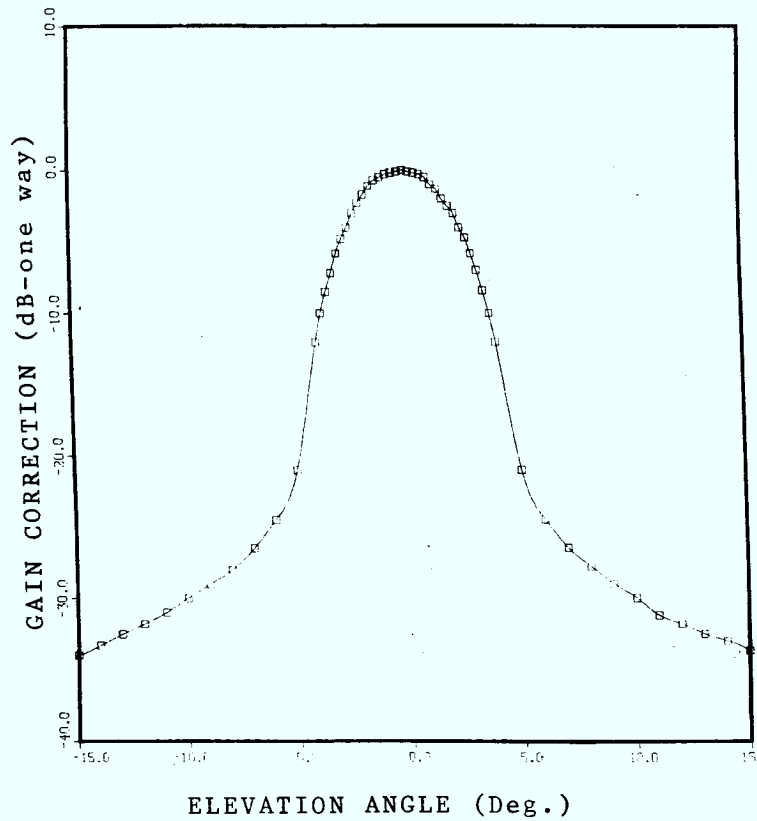


Figure 12 - S-Band Antenna Elevation Pattern.

X-BAND: 9.1 GHZ POL: VERTICAL

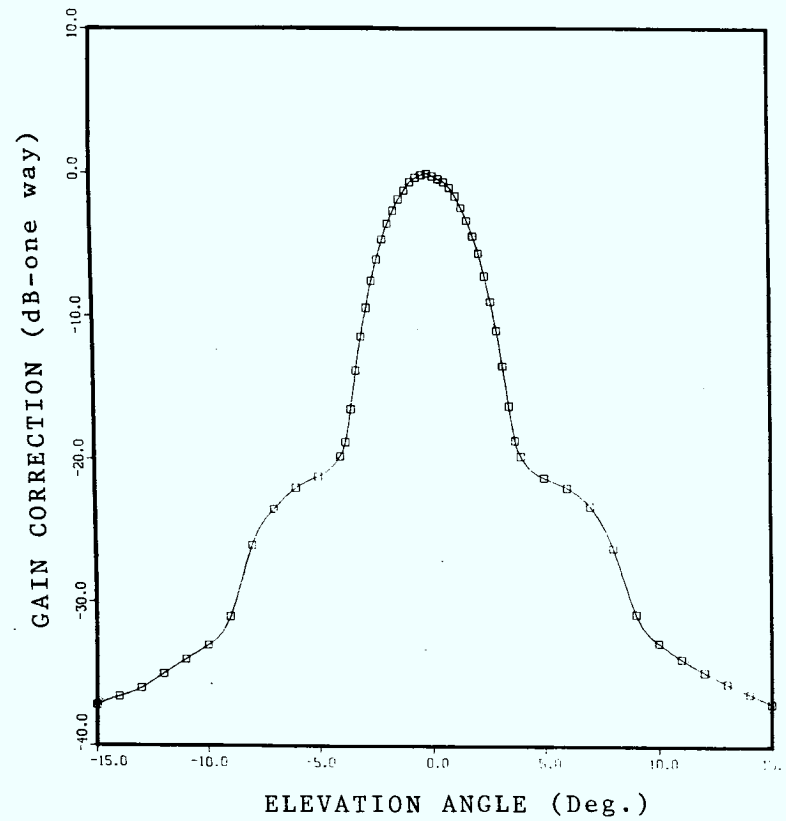


Figure 13 - X-Band Antenna Elevation Pattern.

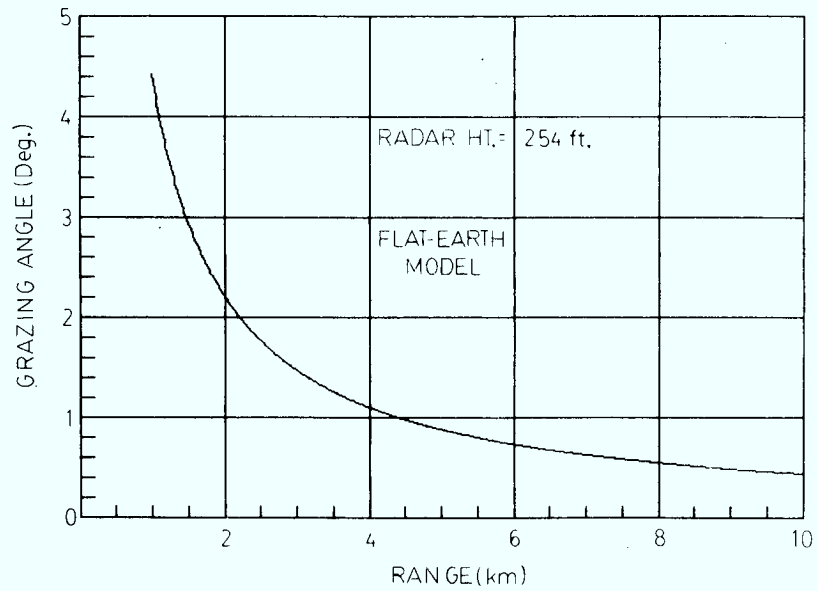


Figure 14 - Grazing Angle as a Function of Range for a Radar Height of 254 ft

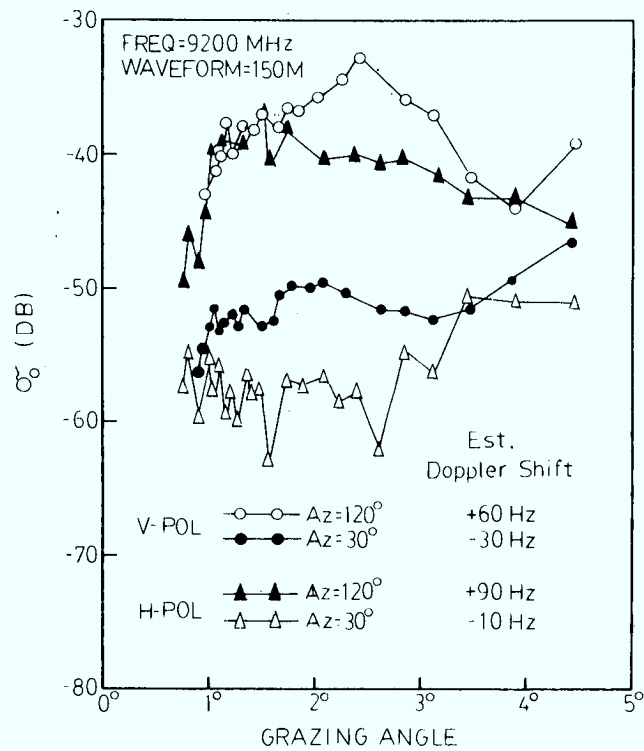


Figure 15 - Typical σ_0 vs Grazing Angle Plot for X-band Data

the returns from the same direction between the cases of vertical polarization and horizontal polarization for X-band transmissions. This means that the vertical-to-horizontal polarization ratio of σ_0 , expressed in dB, is relatively small for X-band sea-clutter.

In Figure 16, plots of σ_0 vs grazing angle for typical S-band experiments are given. As in the X-band results, the up-wind to down-wind ratio of σ_0 is fairly high. In this particular case, this ratio is about 7 dB. The vertical-to-horizontal ratio of σ_0 for S-band data is higher than that for X-band data, in the order of 10 dB.

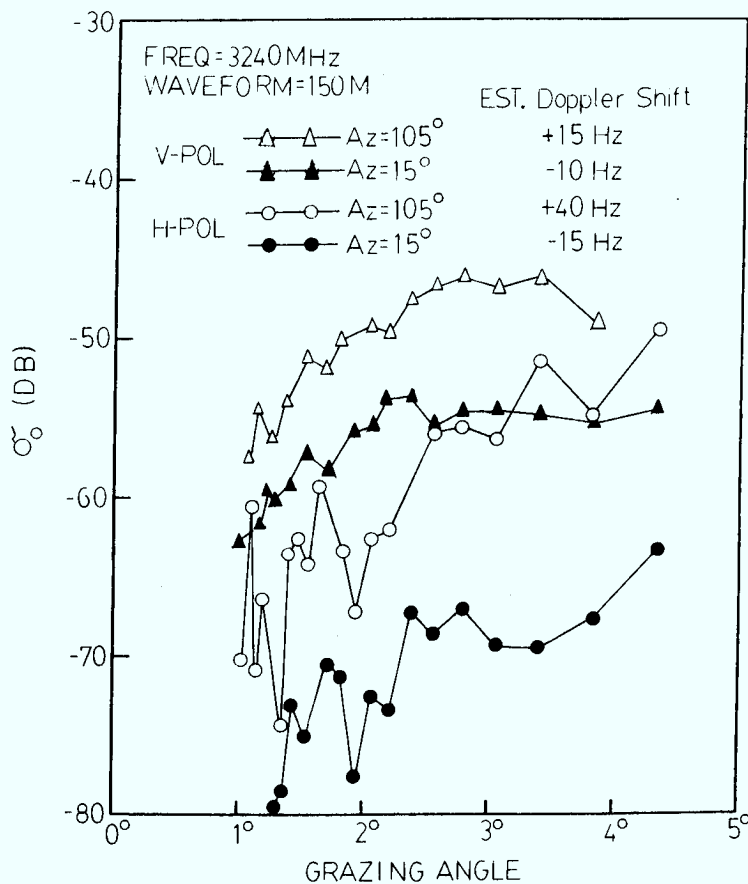


Figure 16 - Typical σ_0 vs Grazing Angle Plot for S-Band Data

In Figure 17, plots are given of σ_0 vs grazing angle for L-band experiments. The upwind-to-downwind ratio of σ_0 is small for L-band, vertically polarized data. This observation is based on the relatively consistent sea-clutter magnitude for L-band data with both positive and negative Doppler shifts. Figure 18 shows the σ_0 vs range plot for two L-band, vertical polarization experiments. Trace A is derived from data

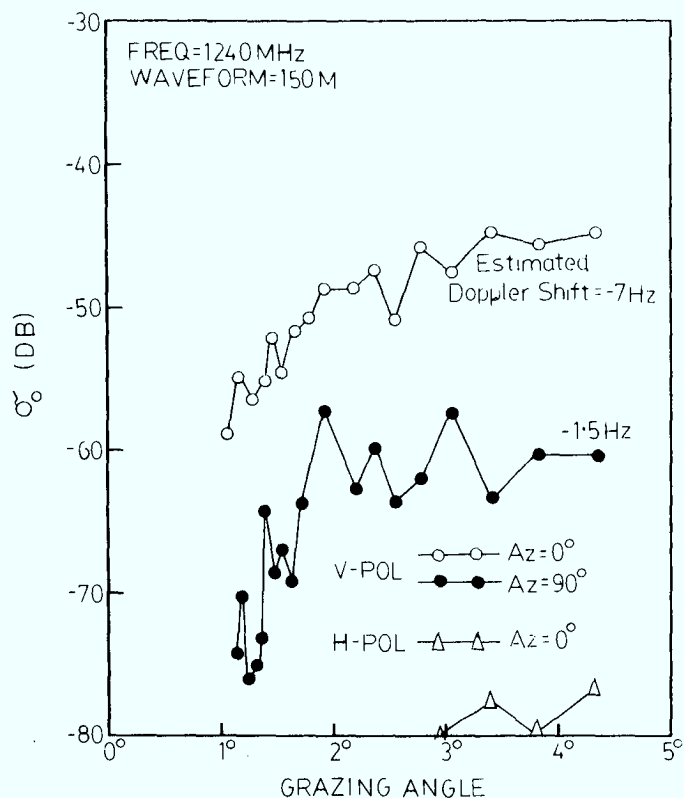


Figure 17 - Typical σ_0 vs Grazing Angle Plot for L-band Data

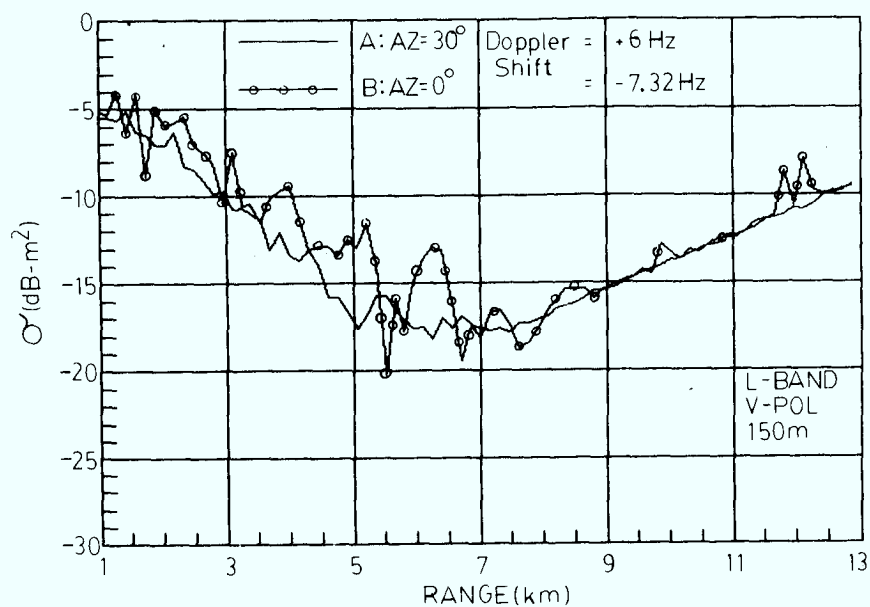


Figure 18 - L-band Sea Clutter in Up-wind, Down-wind Conditions

at a look direction of 30 degrees. The typical Doppler shift in this experiment is about +6 Hz. Trace B of Figure 18 represents σ as a function of range for a similar experiment performed a few days later. The weather conditions around the radar site were similar for both experiments. The averaged Doppler shift for this experiment is -7.32 Hz. If we consider the data with positive and negative Doppler shifts represent approximately data for up-wind and down-wind conditions, the ratio between the estimated σ_0 values in these two cases would give an approximate up-wind to down-wind ratio of σ_0 . There does not seem to be a significant difference in clutter magnitudes between the two cases. This is observed in most L-band, vertical polarization experiments. Consequently, the observed upwind-to-downwind ratio of σ_0 for L-band sea-clutter is relatively small.

Figure 19 superimposes the σ vs range results of five different look directions for an L-band vertical polarization experiment. The averaged Doppler shifts for the data in Figure 19 are indicated for each curve. At 0° azimuth, the Doppler shift is about -7.32 Hz. This translates into a radial wave velocity of 2 mph. At 90° azimuth, the Doppler shift is -1.46 Hz, corresponding to a velocity of 0.39 mph. This implies that, at this azimuth, the look direction is approaching the cross-wind direction. The magnitude of the sea-clutter return in this direction is seen to reduce substantially as the look direction approaches the cross-wind direction. Compared to those of the X-, and S-bands, the upwind-to-crosswind ratio of σ_0 for L-band is higher.

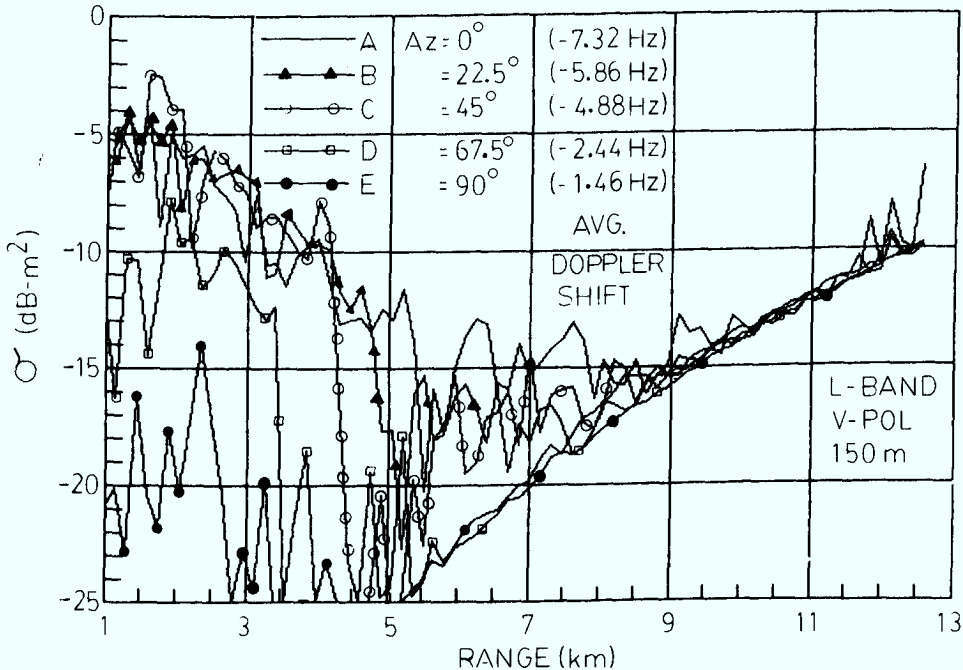


Figure 19 - L-band σ vs. Range Profile for Five Look Directions

Comparison among L-band vertical and horizontal data indicates that the vertical-to-horizontal polarization ratio of σ_0 is quite high for L-band sea-clutter. An average value of 35 dB was observed over experiments performed within a very short time span of one another, as can be seen from Figure 17.

The sea-clutter radar cross section coefficient analysis results are correlated with the wave buoy data. Most of the wave parameters, however, do not show a significant degree of correlation to the results, except (a) the number of waves and (b) the wave period. The number of waves is approximately inversely proportional to the parameters related to the wave period. In most experiments, when the wave period of the water wave decreases, the measured σ_0 value of the data tends to increase.

4.1.3 Comparison of Sea-Clutter σ_0 with Published Data

The wave buoy data recorded during the experimental period indicated that the prevailing sea state was between 1 and 2. It is of interest to find how the measured σ_0 values compare with previously published data. It is always difficult to compare two sets of data without knowing the precise conditions under which the data were obtained. Nevertheless, such comparisons serve to bring out any unusual characteristics in the present set of data which may require more detailed investigation.

In Figure 20, the σ_0 values of X-band sea-clutter computed from the North Truro data are compared to data in Nathanson [5] as well as those derived from the Georgia Institute of Technology (GIT) sea-clutter model [7]. The calculation used in the GIT model employed identical radar parameters as those of the Lincoln Laboratory radar. The mean wave height used is 0.33m which is approximately equal to the averaged value provided by the wave buoy data. It can be seen that, for X-band, the data agreed with the published data reasonably well. There are not sufficient data to show an averaged curve for each set of experimental conditions. The shaded area represents the range of σ_0 values observed over all the experiments which had detectable sea-clutter components (above noise level).

In Figure 21, similar comparisons are shown for S-band data. In this case, however, the vertical-to-horizontal polarization ratio of σ_0 is greater for the North Truro data than that of the published data.

In Figure 22, similar comparisons are shown for L-band data. In this case, the vertical-to-horizontal polarization ratio of σ_0 is significantly higher than in the S-band and X-band cases. Because of the limited data base, it is not possible to verify these observations at higher sea-states. It is possible that propagation conditions such as multipath could be the cause.

4.2 Spectral and Temporal Correlation Analyses

Spectral analysis of sea-clutter processes is useful in measuring

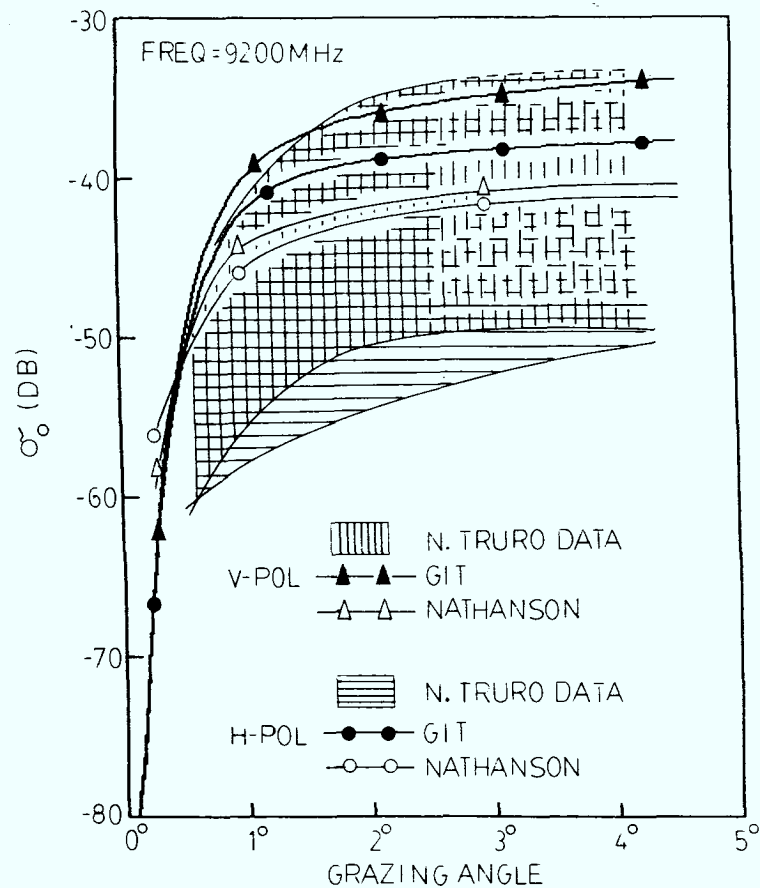


Figure 20 - Comparison of N. Truro X-band Sea-Clutter σ_0 with Published Data.

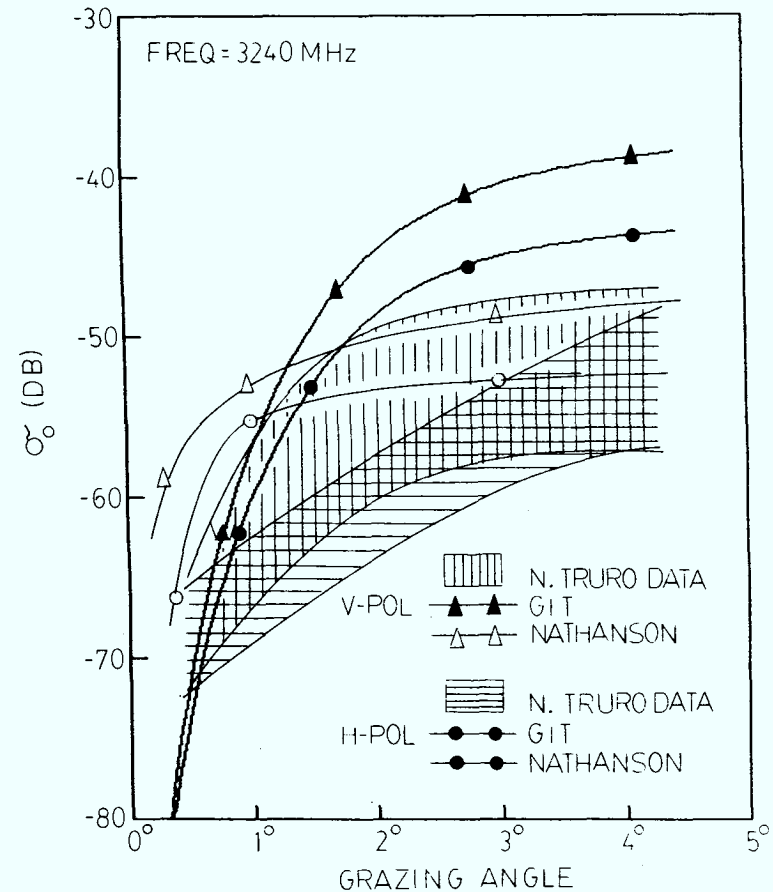


Figure 21 - Comparison of N. Truro S-band Sea-Clutter σ_0 with Published Data.

their decorrelation time and in the evaluation of certain signal processing performance such as moving target indicator (MTI) filters. The decorrelation time of sea-clutter processes is important in assessing the performance of certain coherent radar image processing algorithms in sea-clutter background. The relationship between the sea-clutter spectra and many meteorological parameters such as wind direction, wind speed and sea state are still not well established. Consequently, any additional observations will add new insight to radar sea-clutter behaviours.

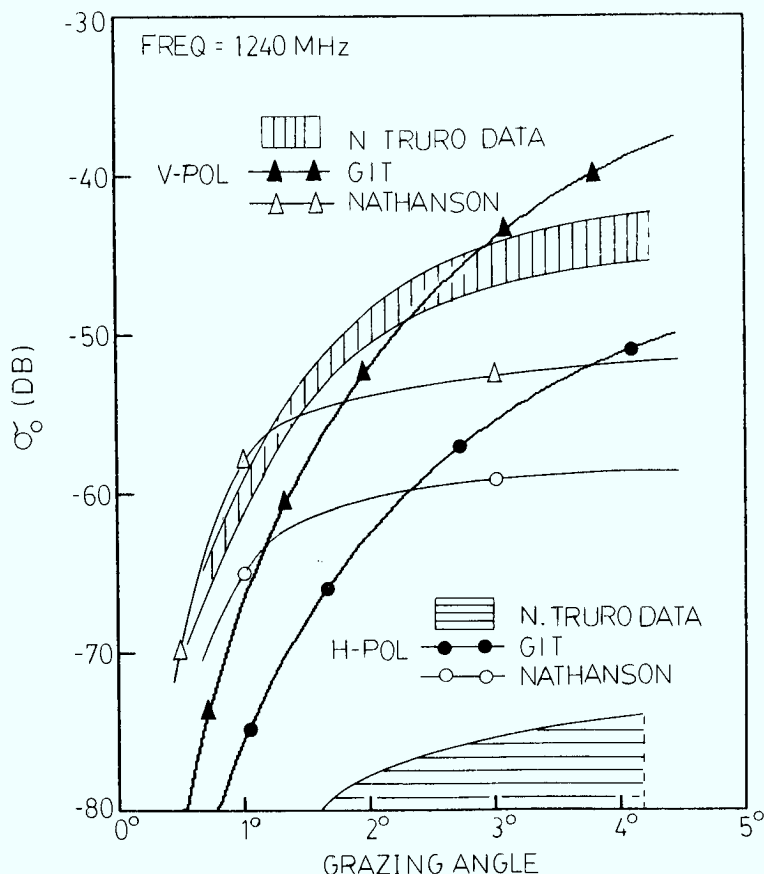


Figure 22 - Comparison of L-band Sea Clutter σ_0 with Published Data.

4.2.1 Doppler Shift and Spectral Width of Sea-Clutter

Two spectral parameters are of particular interest, namely, the Doppler frequency shift and the spectral width of the sea-clutter spectrum. There are no precise definitions for these two parameters since the sea-clutter spectrum is not a well defined mathematical function. Generally, one can determine the Doppler shift of the sea-clutter spectrum by

measuring the distance between the spectral peak from zero Doppler frequency. The spectral width of the sea-clutter spectrum is usually measured in terms of the distance between half power(3 dB) points on the spectrum. However, these quantities may be difficult to measure when the sea-clutter spectrum is noisy, which would be the case when only relatively short data records are available for spectral calculation. For this reason, two parameters are defined which can be estimated from the computed power spectrum of the sea-clutter data.

The first parameter is the mean Doppler frequency defined as:

$$\bar{f}_D = \frac{\int_{-\infty}^{\infty} f P(f) df}{\int_{-\infty}^{\infty} P(f) df} \quad (9)$$

where $P(f)$ is the power spectral density of the sea clutter, and f is the Doppler frequency.

The other parameter is the standard deviation of the Doppler frequency

$$\sigma_D^2 = \frac{\int_{-\infty}^{\infty} (f - \bar{f}_D)^2 P(f) df}{\int_{-\infty}^{\infty} P(f) df} \quad (10)$$

These two parameters, by themselves and without precise description of the sea-clutter spectrum, have no particular meaning. However, in most cases, they provide a fairly good estimate of the Doppler shift and the spectral width of the observed sea-clutter. In particular, if the sea-clutter spectrum can be approximated by a Gaussian-shaped function:

$$P(n\Delta f) = \exp\left\{-\frac{(n\Delta f)^2}{k\sigma_f^2}\right\} \quad (11)$$

where Δf = sampling interval and k is an arbitrary constant

then \bar{f}_D and σ_D can provide a good estimate of the Doppler shift and the spectral width respectively.

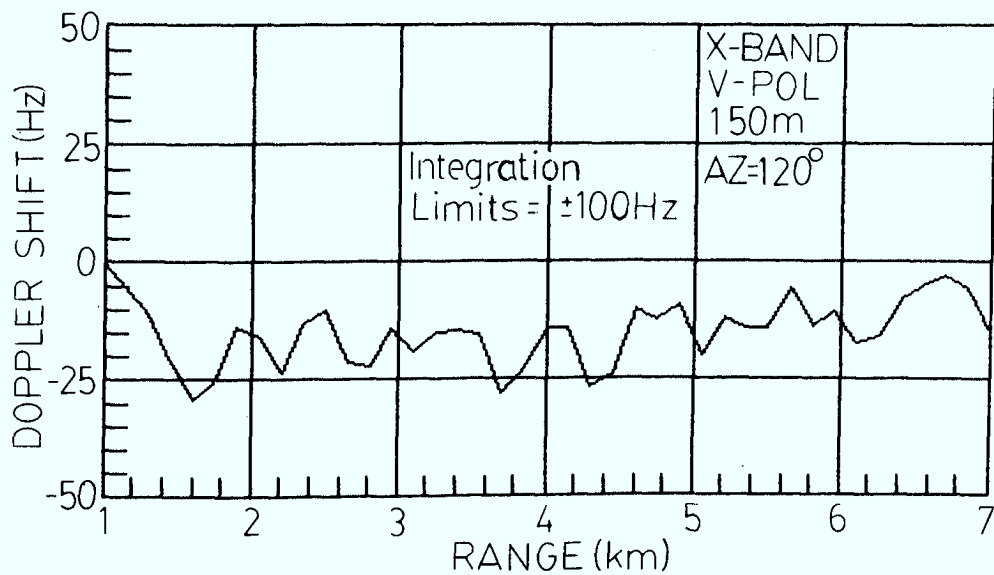
In the analysis, the sea-clutter power spectra are represented by periodograms. Consequently, the integrals in Eqn(9) and (10) are replaced by summations over the Doppler frequency band. These summations are given in Eqn(12) and Eqn(13), respectively.

$$\bar{f}_D = \frac{\sum_{n=0}^{N-1} (n\Delta f) P(n\Delta f)}{\sum_{n=0}^{N-1} P(n\Delta f)} \quad (12)$$

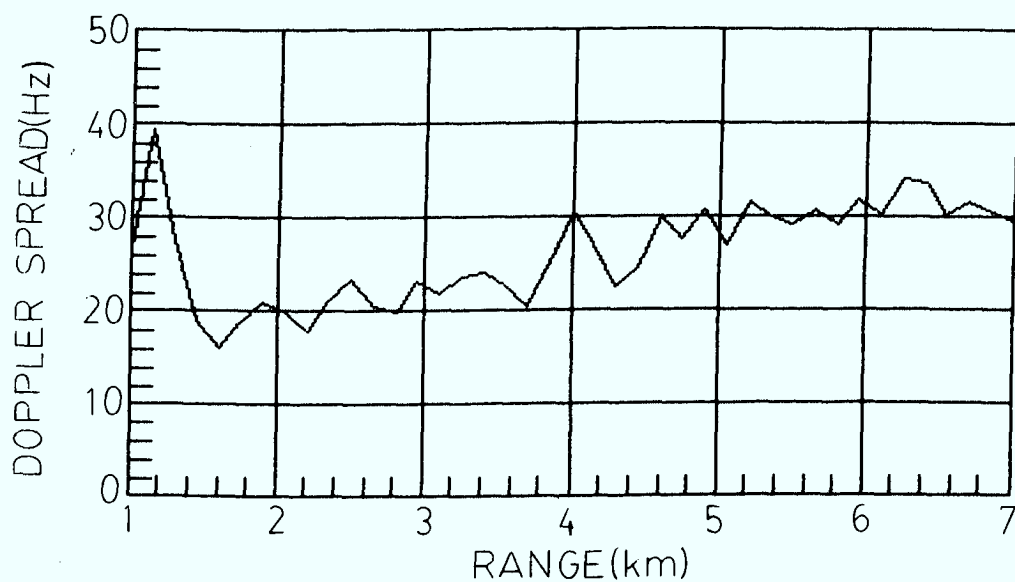
$$\sigma_D^2 = \frac{\sum_{n=0}^{N-1} (n\Delta f - \bar{f}_D)^2 P(n\Delta f)}{\sum_{n=0}^{N-1} P(n\Delta f)} \quad (13)$$

In order that the bias introduced by the receiver noise component to the estimates be minimized, the summation limits are restricted to the upper and lower limits of the Doppler frequency cells which contain the visible sea-clutter spectrum, (i.e., the frequency region in which the sea-clutter power is above mean receiver noise level). These limits are determined at the data scanning stage.

Figure 23a and 23b show the estimated mean Doppler shift and the standard deviation of the sea-clutter data, respectively, for an X-band, vertical polarization experiment. The waveform is 150 m, and the look direction is 120 degrees. Data within the range interval from 1 km to 4.6 km were selected for analysis because the data in this range interval have higher clutter-to-noise ratio than those at longer range. The average (over all range cells) Doppler shift for the sea-clutter in this experiment is approximately -22 Hz, and the standard deviation is approximately 20 Hz. A typical spectrum is shown in Figure 24, for an arbitrarily chosen range cell at R=2050m. The Doppler shift for data at this range is -16 Hz, and the standard deviation is 20 Hz(determined by Eqn(12) and (13)). By visual inspection of Figure 24, the Doppler shift and the 3 dB spectral width are approximately determined to be -16 Hz and 43 Hz(about twice the standard deviation), respectively. This relationship have been observed fairly consistently over most data from the North Truro experiment. Thus the mean and standard deviation of the sea-clutter periodogram give a fairly good estimate of the mean Doppler shift and 3dB spectral width of the sea-clutter.



(a) Average Doppler Shift



(b) Standard deviation of Doppler shift.

Figure 23 - Mean and Standard Seviation of an X-band,
Vertical-polarization Sea-clutter spectrum

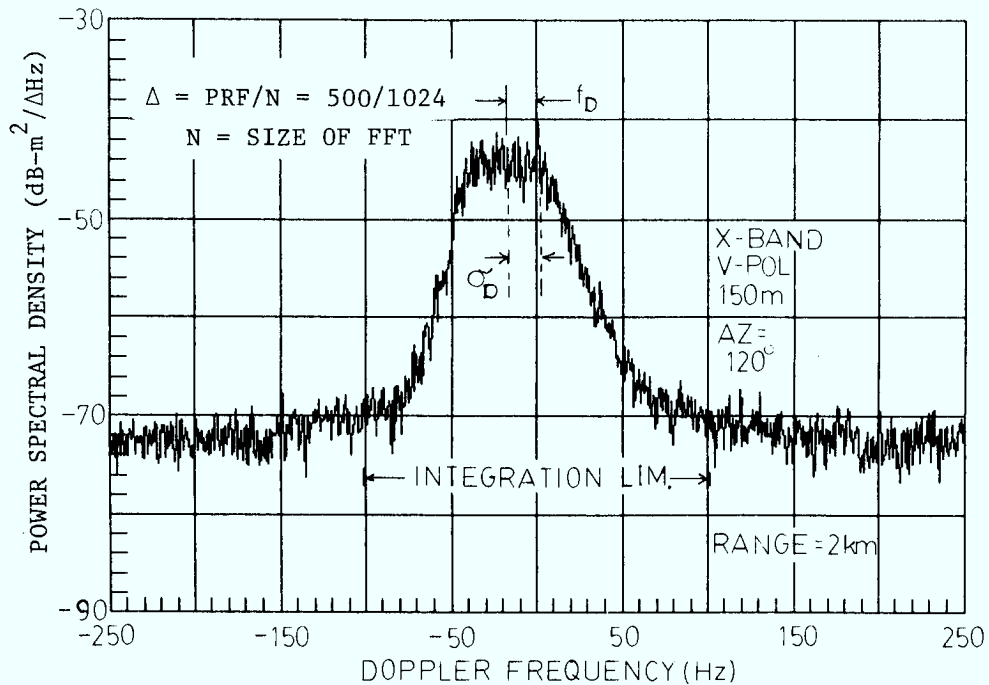


Figure 24 - Doppler-shift and Spread of Sea-Clutter Spectrum

4.2.2 Sea-Clutter Spectra Observed at Different Look Directions

In Figure 25, sea-clutter spectra are shown for an X-band experiment. Trace A and B show the sea-clutter spectra corresponding to up-wind conditions, and trace C corresponds to a down-wind condition. These spectra show that when the sea-clutter has a positive Doppler shift (up-wind condition), or a negative Doppler shift (down-wind condition), the spectrum becomes asymmetrical and has a longer tail in the direction of the Doppler shift. In the cross-wind direction, the sea-clutter spectra tend to be more symmetrical.

In Figure 26, the sea-clutter spectra are shown for an S-band experiment. Similar spectral behaviours were observed as in the X-band experiments. These observations are quite consistent for S-band data with at least a moderate amount of sea-clutter components.

In Figure 27, the sea-clutter spectrum is shown for an L-band experiment. The double peak in the spectrum was observed frequently. These two peaks have opposite Doppler shifts. This may be explained by the wave facet theory. The ensemble of wave facets may have a mean group velocity, however, individual wave facets are often observed to be moving forward and receding alternately. Doppler peaks are observed less often in X-band and S-band data. This could be a result of the returns from

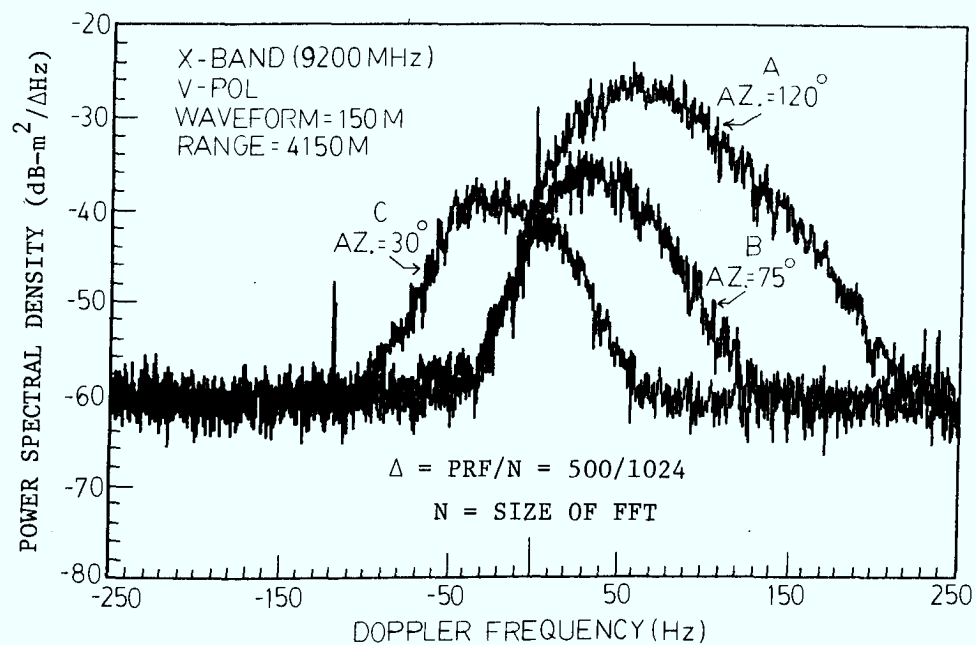


Figure 25 - X-Band Sea-Clutter Spectra in Up-wind and Down-wind Conditions

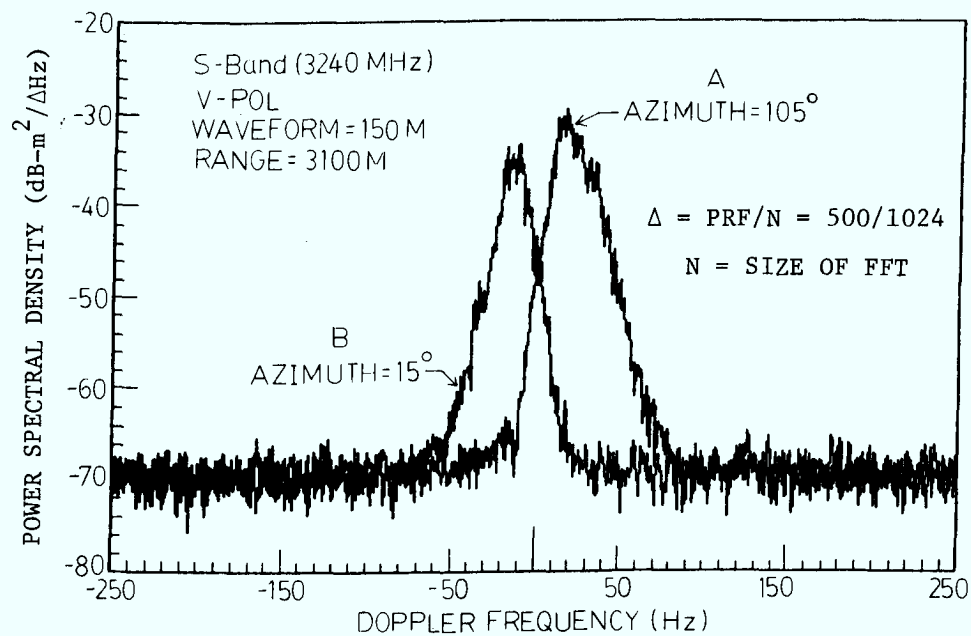


Figure 26 - S-Band Sea-Clutter Spectra in Up-wind and Down-wind Conditions

the finer structure of the waves, such as water droplets, which fill out the spectrum between two peaks. For L-band data, the sea-clutter spectra have a smaller Doppler shift and a narrower Doppler spread. The lowest PRF which can be employed by the Lincoln Laboratory radar is 500 Hz. Subsequent modification to the data acquisition system has enabled the recording of data with a lower effective PRF (by skipping samples). However, this was not available at the North Truro site. As a result, the frequency resolution of the L-band sea-clutter spectra is not as good as that of the S-band and X-band. Consequently, it is not as easy to determine the sea-clutter spectral width as in the cases of X-band and S-band. The autocovariance analysis of the sea-clutter samples can be used to provide the equivalent information.

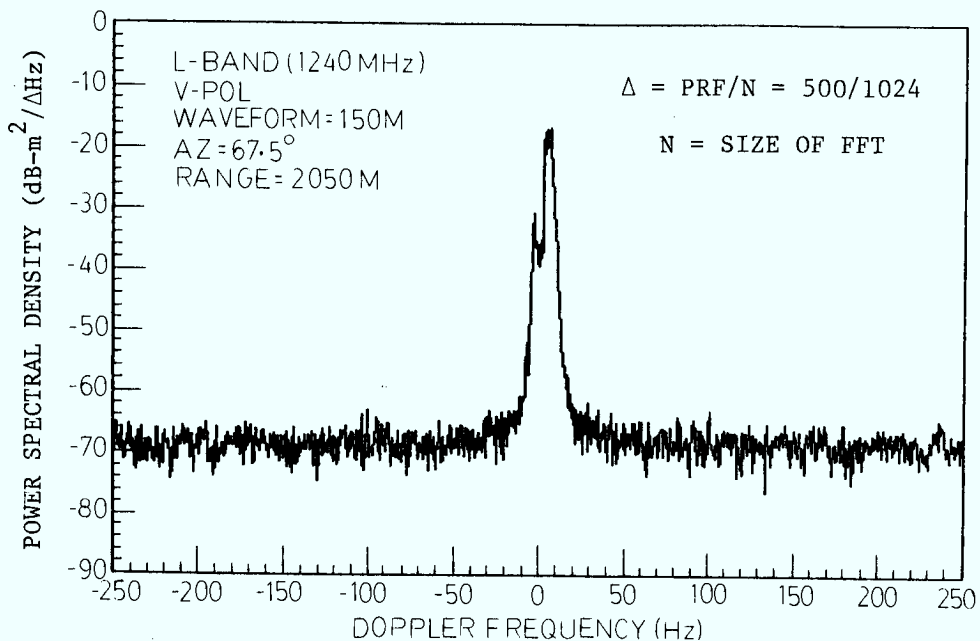


Figure 27 - Typical L-band Sea-Clutter Spectrum

The results of sea-clutter data analysis are correlated with the wind direction and velocity measurement data. Unfortunately, the wind direction and velocity measurements were only set up at the radar site. Consequently, the measured wind data bore little relationship with the actual wind direction and velocities several kilometers offshore. This discrepancy was borne out by the data recorded during a rain storm. Figure 28 shows the σ vs range plot for an X-band experiment performed while a rain storm was several kilometers off shore. Normally the clutter component in the data would drop off with increasing range. However, in this case the magnitude of the samples increases beyond 5 km. This was, of

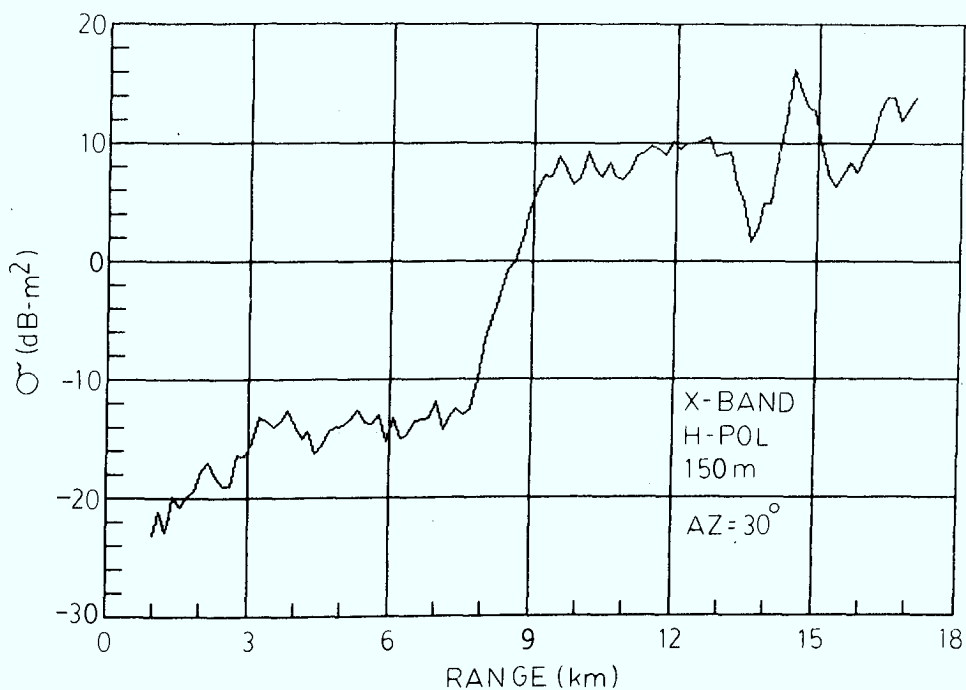


Figure 28 - σ vs Range Plot for a Data Set Containing Rain Clutter

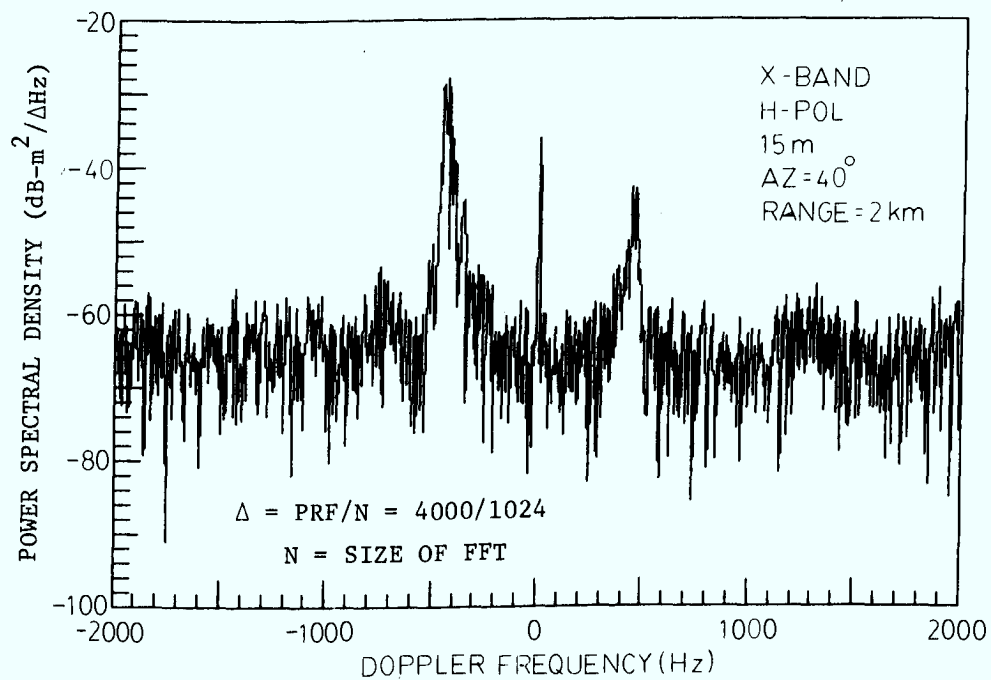


Figure 29 - Spectrum of X-band, Horizontal Polarization Clutter Data Containing Rain Clutter

course, the result of the returns from the rain cloud. Figure 29 shows the spectrum of the data for a particular range cell collected in this experiment. It shows a spectral component centered at about -450 Hz Doppler frequency. This would translate into a velocity 16.4 mph away from the radar. The spike at zero Doppler frequency is the ground return picked up from the antenna sidelobes. A smaller spectral component is also present around zero Doppler. This is the sea-clutter component. The wind velocity recorded at the radar site during this experiment was 1 mph at 250 degrees azimuth. In order for the rain cloud to attain a velocity of 16.4 mph, it must have been driven by a wind velocity much higher than the recorded 1 mph value. The only logical conclusion is that the wind velocity and direction in the vicinity of the rain storm were not the same as those recorded at the radar site. Similar behaviour was observed for vertical polarization experiments.

An interesting feature was noted in some X-band, horizontal polarization spectra. In Figure 29, in addition to the Doppler shift centred at -450 Hz, there is also a component which centred at about +450 Hz. This component seems to drop off with increasing range and was only observed in high resolution, horizontal polarization experiments. Because of the lack of ground-truth, it is not possible to relate this phenomenon to any physical properties of the area being observed by the radar.

4.2.3 Sea-clutter Decorrelation Time

Temporal correlation analysis using the autocovariance function of the clutter samples provides essentially equivalent information to that obtained by spectral analysis. Depending on the objective sought, one method may be preferred over the other.

Let $S_n: \{s_0, s_1, \dots, s_{N-1}\}$ be a complex sequence representing the sea-clutter samples from a certain range cell. The autocorrelation function of S_n is defined as:

$$A_k = \frac{\sum_{n=0}^{N-1} S_n^* S_{n+k}}{\sum_{n=0}^{N-1} S_n^* S_n} \quad (14)$$

where * denotes the complex conjugate

The sea-clutter decorrelation time is defined as the time for the envelope of the autocovariance function to drop to $1/e$ of its peak value, where e is the natural base of logarithm.

It is well known [8] that the autocorrelation function and the power spectrum of a signal form a Fourier Transform pair. Consequently, the auto-correlation function can also be obtained by taking the inverse Fourier transform of the sea-clutter power spectrum. For a zero mean random process, the autocorrelation and the autocovariance functions are identical. After the ground-clutter components are removed from the data, the resulting sea-clutter samples constitute a zero-mean random process. For a symmetrical spectrum centred about the zero Doppler frequency, the auto-covariance function is a real and even function. An asymmetrical sea-clutter spectrum results in a complex autocovariance function. If the spectrum is translated in frequency, the resulting auto-covariance function is simply the product of this real function with a complex sinusoid, $\exp(\pm j\omega_0\tau)$, where ω_0 is the angular frequency shift, and τ is the time lag. The sign in the complex sinusoid is associated with the direction of the frequency shift. For a frequency shift in the positive Doppler direction, the exponential is $\exp\{-j\omega_0\tau\}$. For a frequency shift in the negative Doppler direction, the exponential is $\exp\{+j\omega_0\tau\}$.

From the sea-clutter data, it is observed that the 3 dB spectral width of the sea-clutter is approximately equal to the inverse of twice the decorrelation time. The Doppler shift of the sea-clutter spectrum may be determined approximately by the inverse of the period of the modulating complex sinusoid. Figure 30 shows the autocovariance function of a data set from an S-band experiment. The corresponding spectrum of this data set is shown in trace A of Figure 26. The decorrelation time is approximately 29 msec, which gives an estimated 3 dB spectral width of about 17 Hz. The period of the modulating sinusoid is approximately 49 msec. This gives an estimated Doppler shift of 20.4 Hz. These figures agree very well with the result of spectral analysis shown in Figure 26.

Table III summarizes the spectral parameters and the temporal decorrelation characteristics of the North Truro sea-clutter data for X-, S- and L-bands.

TABLE III: Spectral and Decorrelation Characteristics of Cape Cod Sea-Clutter Data.

BAND	RANGE OF DOPPLER SHIFT	3 dB SPECTRAL WIDTH	DECORRELATION TIME
X	0 - 100 Hz	10 - 65 Hz 40 Hz typical	10 msec
S	0 - 25 Hz	5 - 20 Hz 10 Hz typical	50 msec
L	0 - 10 Hz	5 Hz typical	150 msec

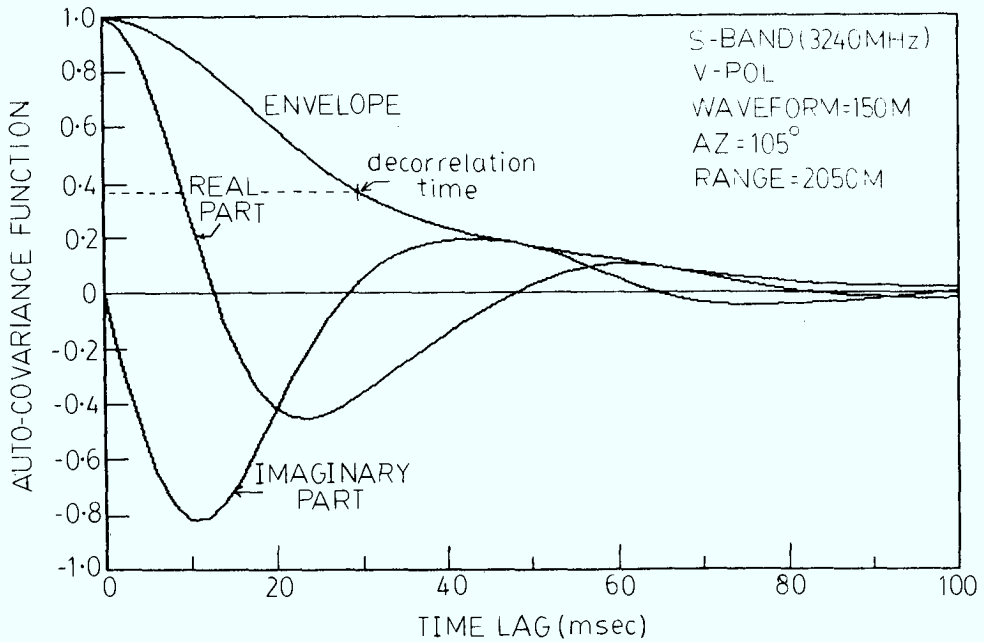


Figure 30 - Auto-covariance Function of an S-band Sea Clutter Data Experiment

4.3 Statistical Analysis

The statistical properties of sea-clutter processes are of interest to radar designers for the prediction of detection and false-alarm rate performances of radars. Much work has been done and reported in the literature[10]-[15]. However, results vary and appear to be dependent on radar system parameters. In this work, the analysis is focused on finding a suitable mathematical model that will give data statistically similar to the observed clutter data. Three models are considered, namely, the Rayleigh, Weibull and log-normal models. The mathematical descriptions of these models are given as follows:

$$\text{Rayleigh: } p(x) = \frac{2x}{\alpha} \exp\left(-\frac{x^2}{\alpha}\right)$$

$$\text{Weibull: } p(x) = n \left(\frac{x^{n-1}}{\alpha}\right) \exp\left(-\frac{x^n}{\alpha}\right) \quad (15)$$

$$\text{Log-Normal: } p(x) = \frac{1}{x\sigma(2\pi)^{\frac{1}{2}}} \exp\left[-\frac{(\ln x - m)^2}{2\sigma^2}\right]$$

$$0 \leq x \leq \infty$$

where α , n , σ and m are model parameters to be estimated from the clutter data.

4.3.1 Estimation of Clutter Model Parameters

The first and second moments of the sea-clutter data are computed from the sample mean and sample variance[16] of the sea-clutter data. They are used to estimate the parameters for the statistical models in Eqn(15).

The first and second moments of a random process are defined in Eqn(16) and Eqn(17), respectively.

$$\langle x \rangle = \int_0^{\infty} x p(x) dx \quad (16)$$

$$\langle x^2 \rangle = \int_0^{\infty} x^2 p(x) dx \quad (17)$$

For a Rayleigh process, only the first moment is required to estimate the parameter. Substituting the Rayleigh probability density into Eqn(16) and integrating by parts yields:

$$\langle x \rangle_R = \int_0^{\infty} \frac{2x^2}{\alpha} \exp\left(-\frac{x^2}{\alpha}\right) dx = \frac{1}{2}(\pi\alpha)^{\frac{1}{2}} \quad (18)$$

from which the parameter α is given as:

$$\alpha = \frac{4}{\pi} \langle x \rangle_R^2 \approx \frac{4}{\pi} (\text{sample mean})^2 \quad (19)$$

For a Weibull process, both the first and second moments are required to evaluate parameters α and n . The first and second moments of Weibull process are given by Eqn(20) and Eqn(21) respectively.

$$\langle x \rangle_W = \int_0^{\infty} \frac{x^n}{\alpha} x^{n-1} \exp\left(-\frac{x^n}{\alpha}\right) dx \quad (20)$$

$$\begin{aligned}
&= \frac{1}{\alpha^n \Gamma(\frac{1}{n}+1)} \\
\langle x^2 \rangle_W &= \int_0^\infty n \frac{x^{n+1}}{\alpha} \exp(-\frac{x^n}{\alpha}) dx \\
&= \alpha^{\frac{2}{n}} \Gamma(\frac{2}{n}+1)
\end{aligned} \tag{21}$$

where $\Gamma(\cdot)$ is the Gamma function

The parameters α and n are obtained by solving Eqn(20) and Eqn(21) simultaneously. Squaring both sides of Eqn(20) and dividing by Eqn(21) yields:

$$\frac{\langle x \rangle_W^2}{\langle x^2 \rangle_W} = \frac{[\Gamma(\frac{1}{n}+1)]^2}{\Gamma(\frac{2}{n}+1)} \approx \frac{(\text{sample mean})^2}{(\text{sample 2nd moment})} \tag{22}$$

The solution to this transcendental equation yields the parameter n , and α is found by substituting n into either Eqn(20) or Eqn(21). The solution to Eqn(22) is obtained numerically using Newton's method[17].

The first and second moments of a log-normal process are given by Eqn(23) and Eqn(24), respectively.

$$\begin{aligned}
\langle x \rangle_L &= \int_0^\infty \frac{x}{x\sigma(2\pi)^{\frac{1}{2}}} \exp\left[-\frac{(\ln x - m)^2}{2\sigma^2}\right] dx \\
&= \exp\left(\frac{2m+\sigma^2}{2}\right)
\end{aligned} \tag{23}$$

$$\begin{aligned}
\langle x^2 \rangle_L &= \int_0^\infty \frac{x^2}{x\sigma(2\pi)^{\frac{1}{2}}} \exp\left[-\frac{(\ln x - m)^2}{2\sigma^2}\right] dx \\
&= \exp[2(m+\sigma^2)]
\end{aligned} \tag{24}$$

Parameters σ and m are obtained from the following set of equations:

$$\begin{aligned}\sigma^2 &= \frac{1}{2} \ln[\langle x^2 \rangle_L] - m \approx \frac{1}{2} \ln(\text{sampled 2nd moment}) - m \\ m &= \ln[\langle x \rangle_L] - \frac{\sigma^2}{2} \approx \ln(\text{sample mean}) - \frac{\sigma^2}{2}\end{aligned}\quad (25)$$

The detailed derivation of the model parameters for the Rayleigh, Weibull and log-normal processes is given in APPENDIX B.

4.3.2 Chi-Square Goodness of Fit of Clutter Models

The sea-clutter data are subjected to statistical tests based on the above three models. The emphasis is not on requiring the data to pass the statistical tests, but rather, on the relative goodness of fit of the sea-clutter data to the assumed models. The criterion for comparison is the parameter χ^2 of the Chi-square goodness of fit test[18].

The sea-clutter samples are used to form an amplitude histogram. The amplitude histogram is divided into K regions of equal probability, $1/K$, based on the assumed model. The parameter χ^2 is computed as:

$$\chi^2 = \sum_{i=1}^K \frac{(f_i - \frac{N}{K})^2}{(\frac{N}{K})} \quad (26)$$

where f_i = observed frequency of occurrence in the i th region, and
 N = total number of amplitude samples forming the histogram.

In the usual Chi-square goodness of fit test, the value χ^2 is computed and compared to a threshold value based on the so-called level of significance. In our work, we use χ^2 as a measuring index to determine the relative goodness of fit of the sea-clutter data to the statistical models. A value of $K = 120$ was used for all tests.

The result of the Chi-square goodness of fit test for the sea-clutter data of an X-band, vertical polarization experiment is shown in Figure 31. The waveform resolution is 150m. The abscissa represents the range cell number starting at 1 km as cell No. 1. Each range cell represents a 150m increment. The solid curve represents the χ^2 values computed for the data from each range cell for the Rayleigh model. The dotted curve represents that of the log-normal model. It can be seen that this data set has a much better fit to the Rayleigh model than to the log-normal model. The same set of data were also subject to the Weibull model test, however, the result is very close to that of the Rayleigh model.

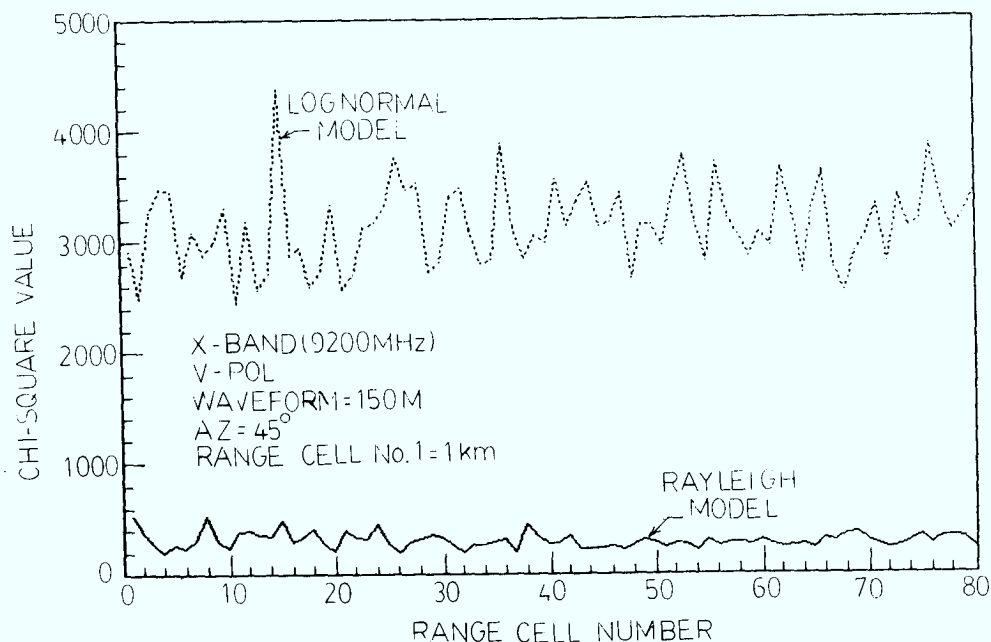


Figure 31 - Chi-Square Goodness of Fit for Vertically Polarized, Low-Resolution, X-Band Sea-Clutter Data

In Figure 32, results are given of the Chi-square goodness of fit test for an X-band, horizontal polarization experiment. All the parameters except for the polarization are the same as those in Figure 31. It can be seen that data from a large number of range cells have a better fit to the log-normal model than to a Rayleigh model. Similar results were observed for S-band data, as shown in Figures 33 and 34 respectively. It is difficult to verify these observations for the L-band, horizontal polarization data because of the extremely low level of returns. Consequently, most of the L-band, horizontal polarization data are receiver noise dominant and presents a good fit to the Rayleigh model.

In Figure 35, results of the Chi-square goodness of fit test are shown for an X-band, horizontal polarization experiment. The waveform resolution is 15m. It shows a much better fit of the data to the log-normal model than to the Rayleigh model. It appears that, for low sea states (between sea states 1 and 2), the statistical properties of sea-clutter are affected by two parameters, namely, the polarization and the waveform resolution.

Figure 36 and Figure 37 illustrate how well the statistical models fit the data when the Chi-square goodness of fit test indicates a relatively good fit. Figure 36 shows the probability of false alarm, as a

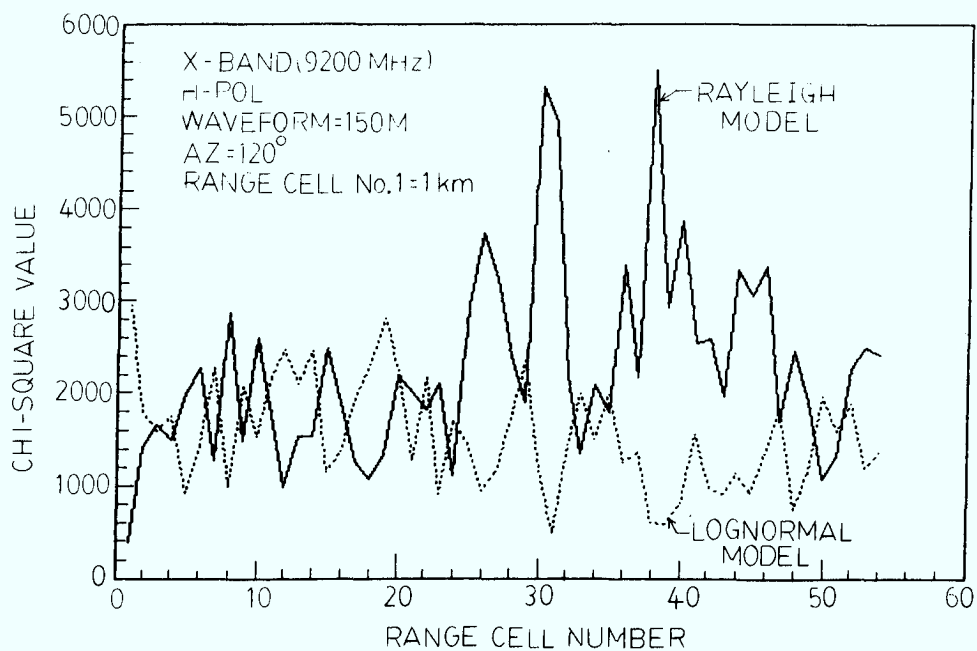


Figure 32 - Chi-Square Goodness of Fit for Horizontally Polarized, Low-Resolution, X-Band Sea-Clutter Data

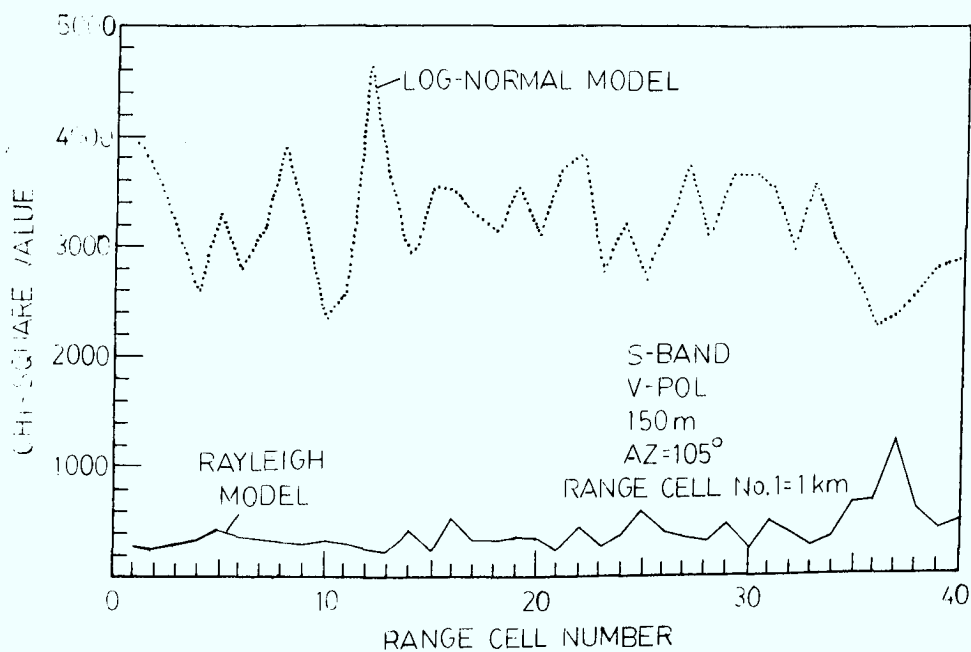


Figure 33 - Chi-Square Goodness of Fit for Vertically Polarized, Low-Resolution, S-Band Sea Clutter Data

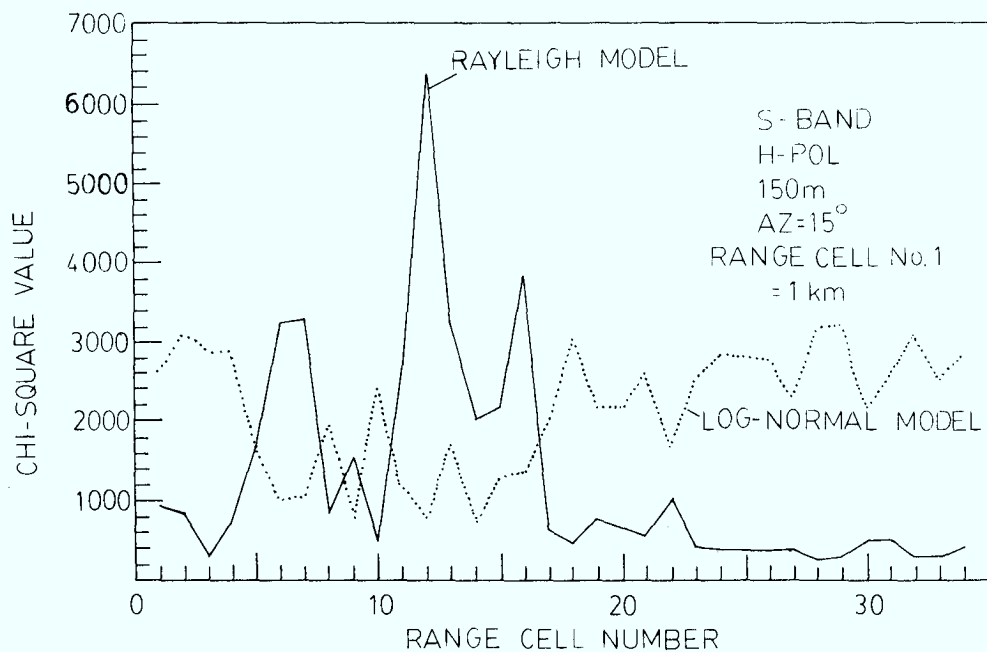


Figure 34 - Chi-Square Goodness of Fit for Horizontally Polarized, Low Resolution, S-Band Sea-Clutter Data

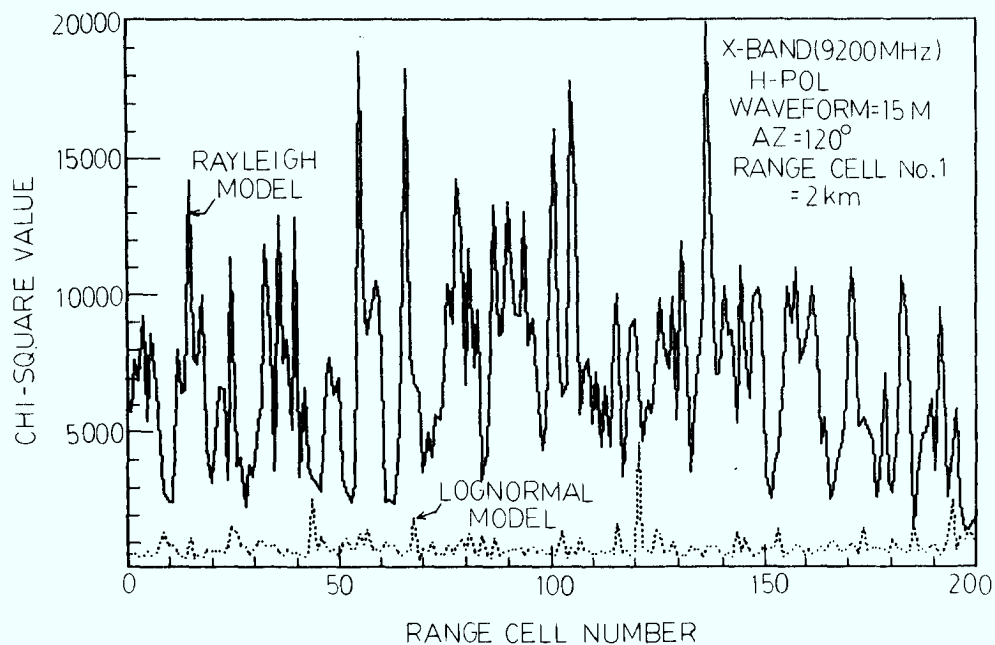
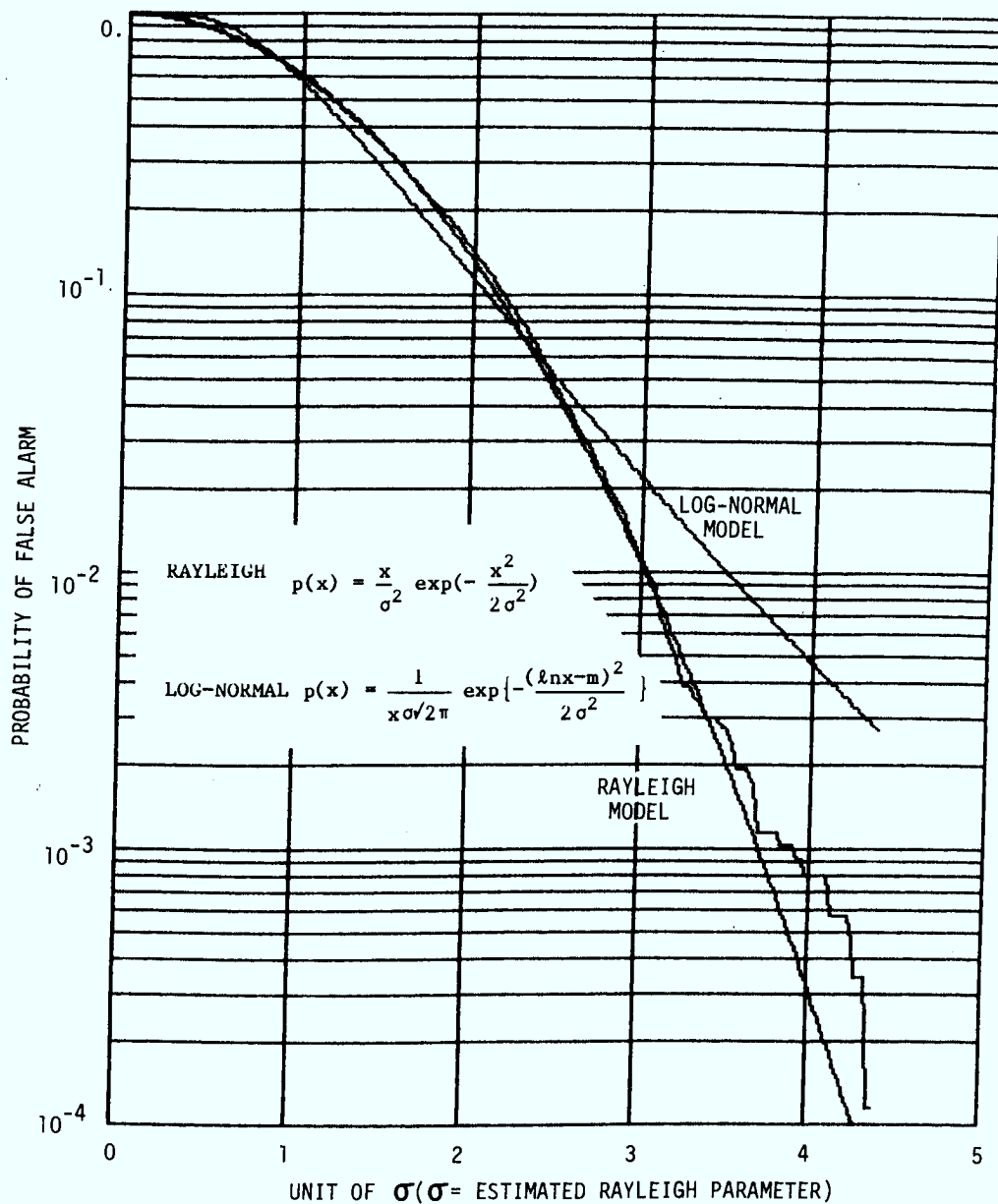


Figure 35 - Chi-Square Goodness of Fit for Horizontally Polarized, High Resolution, X-Band Sea-Clutter Data



TAPE#105030 EXP#5 B=S P=V RR=15M RANGE = 2870M AZ=30°

Figure 36 - Probability of False Alarm as a Function of Threshold for a Data Set fitting the Rayleigh Model

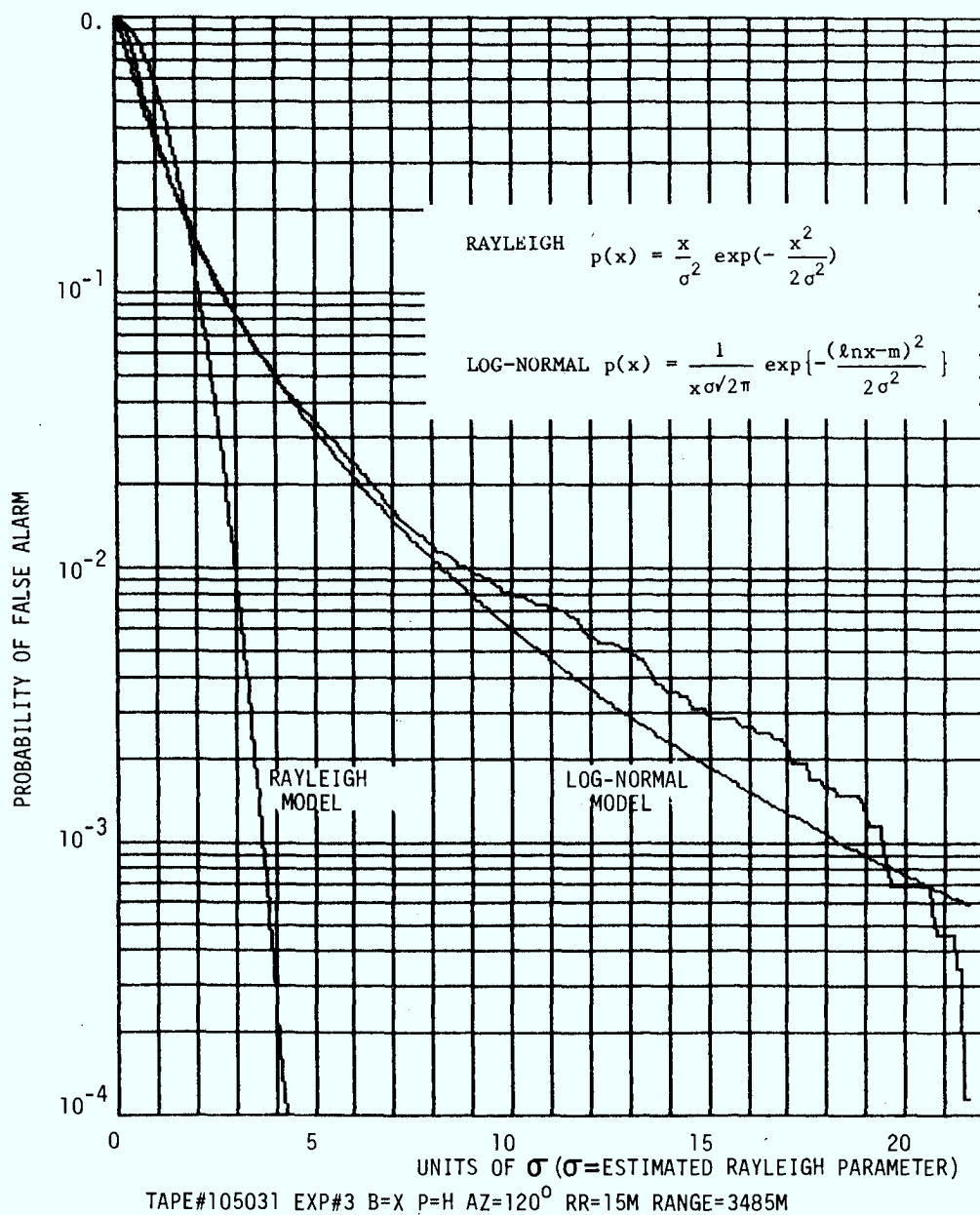


Figure 37 - Probability of False alarm as a Function of Threshold for a Data Set Fitting the Log-normal Model

function of threshold setting, for a data set corresponding to a range cell whose data yield a relatively small χ^2 value for the Rayleigh model. The theoretical Rayleigh false alarm curve with the model parameter estimated from the data is superimposed. It can be seen that the fit is quite good. Figure 37 shows the probability of false alarm as a function of threshold setting, for a data set corresponding to a range cell whose data yield a relatively small χ^2 value in the test for log-normal model. The theoretical log-normal false alarm curves is superimposed on the figure. It indicates a very good fit to the log-normal model. The threshold setting is normalized to the Rayleigh parameter α .

5. SUMMARY OF RESULTS AND RECOMMENDATIONS

5.1 Summary of Results

Even though the data base of the North Truro experiment is relatively limited, some interesting results were observed. These results will be summarized in this section. It should be emphasized that these results pertain to sea-clutter data obtained for grazing angles below 4 degrees under sea states 1 and 2, and they should not be extrapolated to higher sea states without verification with actual data.

(a) Sea-Clutter Radar Cross Section Coefficients

- i) Generally σ_0 of sea-clutter increases with increasing radar frequency.
- ii) Vertical-to-horizontal polarization ratio of σ_0 under calm sea conditions increases with decreasing radar frequency band. At X-band, the vertical-to-horizontal polarization ratio of σ_0 , expressed in dB, is small. This ratio increases substantially at S-band, and it increases even further at L-band.
- iii) For X- and S-bands, the upwind-to-downwind ratio of σ_0 is quite high. However, the upwind-to-crosswind ratio is only marginally higher than the upwind-to-downwind ratio of σ_0 . At L-band, the upwind-to-downwind ratio of σ_0 , expressed in dB, is quite low (about a couple of dBs), but the upwind-to-crosswind ratio is quite high.
- iv) Under calm sea conditions, σ_0 seems to vary inversely with the wave period of the water wave.

(b) Sea-clutter Spectra and Decorrelation Time

- i) For X- and S-band data, sea-clutter spectra appear asymmetrical when the spectrum has a significant Doppler shift. The spectral tail is longer in the direction of the Doppler shift. For L-band data, this effect is less apparent.

- ii) For L-band data at close range, sea-clutter spectra often exhibit double spectral peaks. Double spectral peaks are observed less frequently in S-band and X-band data.
 - iii) No strong correlation was observed between the Doppler shift and spectral spread of sea-clutter data and the wind speed and direction recorded at the time of the experiment near the radar site. A possible explanation is that the data recorded correspond to regions very close to shore, and the water wave motion is more strongly influenced by the direction of ocean current than by local wind velocity. It could also be that the wind direction and speed offshore were different from those at the radar site.
- (c) Sea-clutter Statistics
- i) For low resolution waveforms(150 m), sea-clutter amplitude statistics may be closely modelled by Rayleigh distribution. If Weibull model is used, the parameters estimated from the first two moments of the sea-clutter samples are very close to that of the Rayleigh model.
 - ii) Deviation from the Rayleigh model occurs when high resolution waveform(15 m) or horizontal polarization is employed. However, the polarization dependence of sea-clutter statistics needs to be tested with data for higher sea states.

This set of experiments permits the comparison of sea-clutter characteristics under virtually identical conditions for different polarizations and look directions. Consequently, it provides additional insights into the behaviour of sea-clutter. The differences in the observed upwind-to-downwind ratio, the upwind-to-crosswind ratio, and the vertical-to-horizontal polarization ratio of σ_0 for various frequency bands provide some clues for the identification of the underlying mechanisms of sea-clutter.

The generally observed higher values of σ_0 in upwind direction tend to support the theory that wave facets play a prominent role in sea-clutter. In the up-wind direction the forward wall of sea waves makes a larger angle with the horizontal plane than that of the backward wall. Consequently, it presents a larger effective angle of incidence to the radar, thus producing a stronger return. Also when the significant period of the water wave is small, for the same wave height, the slope which the wave surface makes with the horizontal plane will increase. This again presents to the radar a larger angle of incidence. Analyses of S-band and X-band data support the theory that, at higher frequencies, the finer structure of the water wave, such as water droplets, contributes significantly to the magnitude of the sea-clutter. The relatively small difference between the upwind-to-downwind and the upwind-to-crosswind ratios of σ_0 at S-band and X-band may imply that water droplets play a prominent role in sea-clutter behaviour at higher frequencies. Water droplets re-

flect vertically and horizontally polarized signals of compatible wavelengths equally well. This is consistent with the observed small vertical-to-horizontal polarization ratio of σ_0 for X-band data.

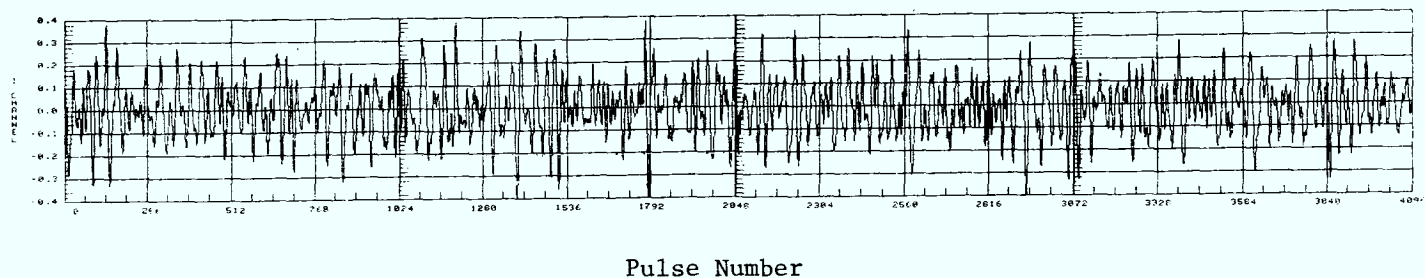
At L-band the sea-clutter seems less sensitive to the fine structure of the water wave and more sensitive to the specular reflection of the signal from the gross wave surfaces. This hypothesis may be used to explain the relatively low upwind-to-downwind ratio of σ_0 at L-band.

One notable result of the analysis of the North Truro sea-clutter data is the increasing vertical-to-horizontal ratio of σ_0 for decreasing frequency. One possible explanation could be the multipath effect. For horizontal polarization, the reflection coefficient for sea water is very close to -1 for a wide range of grazing angles. At lower frequencies and low sea states, the sea surface will behave more like a smooth surface than at higher frequency, thereby creating a more favorable condition for specular reflection. Under the proper conditions, cancellation of the direct and indirect returns could result, thereby producing a much weaker horizontal polarization sea-clutter return. However the limited amount of data available does not permit a more in-depth investigation of possible multi-path effects.

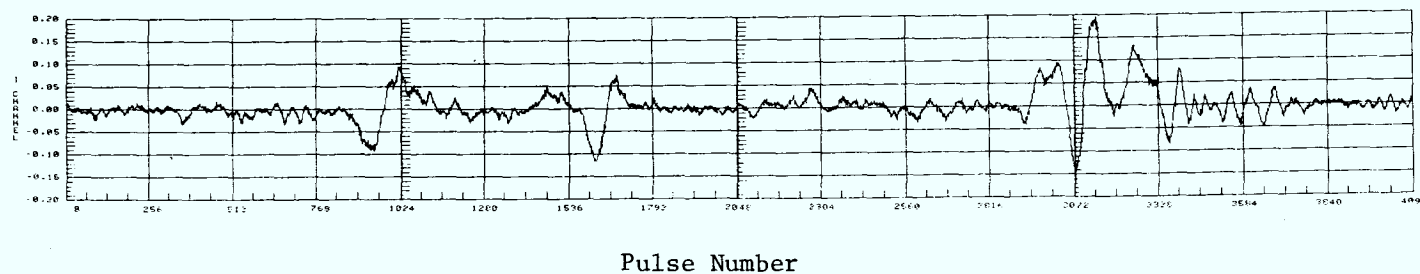
This analysis is also useful in developing signal processing techniques for improving radar performance. The difference in the sea-clutter returns at S- and L-bands, for vertical and horizontal polarizations, may provide a means for improving target detection in sea-clutter, by employing radars with polarization diversity. Generally, for horizontal polarization, the sea-clutter returns are lower in magnitude but are more spiky. Figure 38 compares the I-channel samples of an X-band experiment for vertical and horizontal polarization cases, respectively. The waveform for the horizontal polarization experiment has relatively low amplitude with occasional large spikes. These spikes are what contribute to the log-normal-like behaviour of horizontal polarization sea-clutter. There is a certain periodicity associated with the appearance of the sea spikes. If it is possible to reliably predict the occurrence of these sea spikes, then it might prove to be useful in improving the detection performance of the radar.

For high resolution waveform transmissions, sea-clutter returns exhibit large fluctuation in magnitude among neighbouring range cells. This may present problems when range averaging CFAR's are employed.

Although the relationship between the sea-clutter spectral characteristics and wind velocity could not be observed in these experiments, there are some patterns which can be observed. Generally the sea-clutter spectrum will exhibit a longer tail on the positive Doppler frequency region if it has a positive Doppler shift. This corresponds to the condition where the water wave is travelling towards the radar. In this situation, the front of the wave will experience breaking in its crest, which comprises a large number of water droplets. These water droplets will have



(a) Vertical Polarization.



(b) Horizontal Polarization.

Figure 38 - Comparison of Vertical and Horizontal Polarization Sea-clutter Waveforms. (X-band, 15m Waveform)

a much higher rate of motion than the group velocity of the water wave. Consequently, the observed spectral tail would be longer.

5.2 Recommendations

Some interesting results have been observed by analyzing the North Truro sea-clutter data. However, much work remains to be done before a clear understanding of sea-clutter behaviours can be obtained. Nevertheless, these data point out some of the areas in which improvement can be made if future sea-clutter collection experiments are planned. A list of recommendations which may help to improve data quality in future experiments is given below:

- (a) In future sea-clutter data collection experiments, in order that sea-clutter data of higher sea states can be obtained, a longer experimental period would be desirable. Careful study of the weather pattern of the radar site is also essential.
- (b) Because of the relatively small values of the sea-clutter radar cross section coefficient, long dwell data mode is desirable in order to extract sea-clutter components in the presence of receiver noise and ground clutter interferences from antenna sidelobes.
- (c) More sophisticated wave measurement equipment should be deployed to provide wave direction as well as more accurate ground truth information.
- (d) Wind measuring equipment should be deployed strategically in area of radar illumination to provide more accurate wind direction and speed information.
- (e) For lower radar frequencies such as VHF, UHF and L-band, the PRF should be lowered to provide higher resolution in the sea-clutter Doppler spectra.
- (f) Range extent in which sea-clutter data are collected should be made a function of the magnitude of the sea echo, so as not to collect a large amount of receiver noise samples.
- (g) For shipborne radar applications, sea-clutter should be collected with shipborne radars so as to account for the interaction of ocean waves with the radar platform.
- (h) A phased array antenna system would be useful for the collection of sea-clutter data for spatial correlation studies.

In conclusion, although the data obtained in this particular set of sea-clutter experiments pertain to conditions between sea states 1 and 2,

they provide additional evidences of some of the underlying mechanisms of sea-clutter processes. With more data from future sea-clutter measurements, a more comprehensive picture of the sea-clutter behaviour will eventually emerge.

6. APPENDICES

A SUMMARY OF SEA BUOY DATA

The sea-wave data collected using the ENECOD 949 wave buoy during the North Truro experiment are summarized in Figures A.1 through A.10

B COMPUTATION OF SEA CLUTTER MODEL PARAMETERS

B.1 Rayleigh Processes

The probability density function for a Rayleigh random process is defined as:

$$p(x) = \frac{2x}{\alpha} \exp\left(-\frac{x^2}{\alpha}\right) \quad 0 < x < \infty \quad (\text{B1.1})$$

where

α is the parameter to be estimated from the sampled data of this process

The mean or the first moment is defined as:

$$\langle x \rangle_R = \int_0^{\infty} x p(x) dx = \int_0^{\infty} \frac{2x^2}{\alpha} \exp\left(-\frac{x^2}{\alpha}\right) dx \quad (\text{B1.2})$$

From the table of definite integrals[19], we have:

$$\int_0^{\infty} x^{2n} \exp(-ax^2) dx = \frac{1 \ 3 \ 5 \ \dots (2n-1)}{2^{n+1} a^n} \left(\frac{\pi}{a}\right)^{1/2} \quad (\text{B1.3})$$

Letting $a = \frac{1}{\alpha}$ and $n = 1$ yields:

$$\langle x \rangle_R = \int_0^{\infty} 2ax^2 \exp(-ax^2) dx \Bigg|_{a=\frac{1}{\alpha}}^{n=1} = \frac{1}{2} (\pi\alpha)^{1/2} \quad (\text{B1.4})$$

If a sufficiently large number of samples is taken from a random process, then an unbiased estimate of the first moment can be obtained by computing the sample mean. Hence the Rayleigh parameter α can be approximated by:

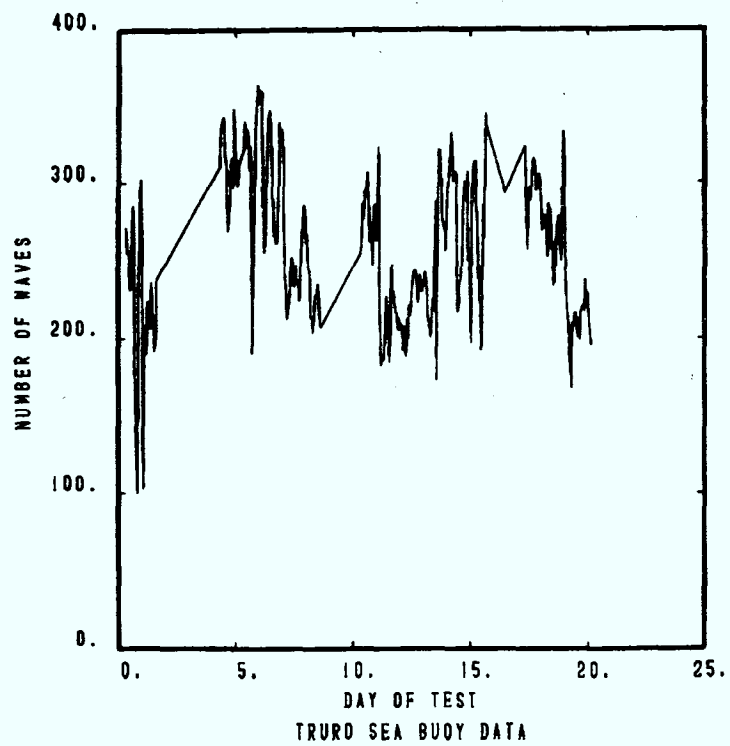


Figure A1 - Number of Waves.

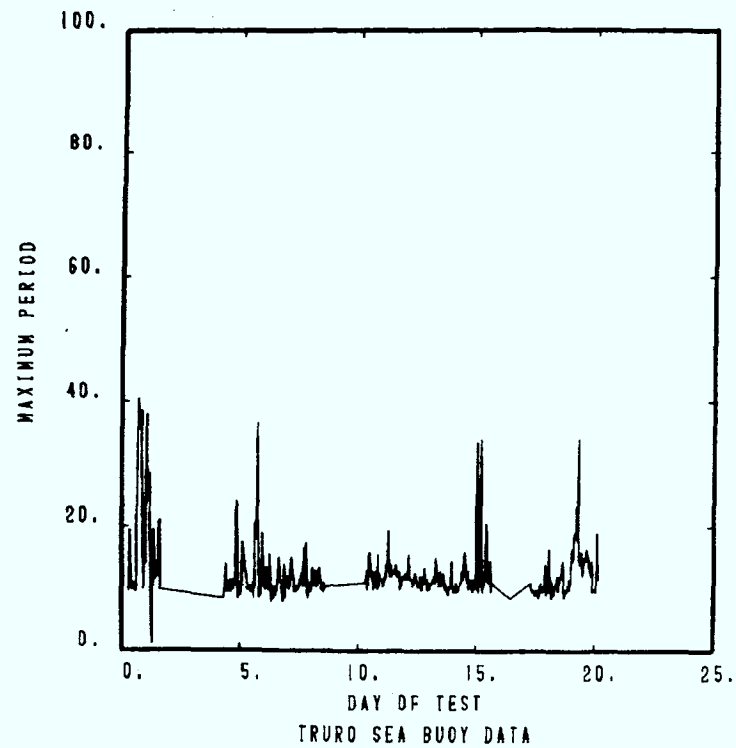


Figure A2 - Maximum Period.

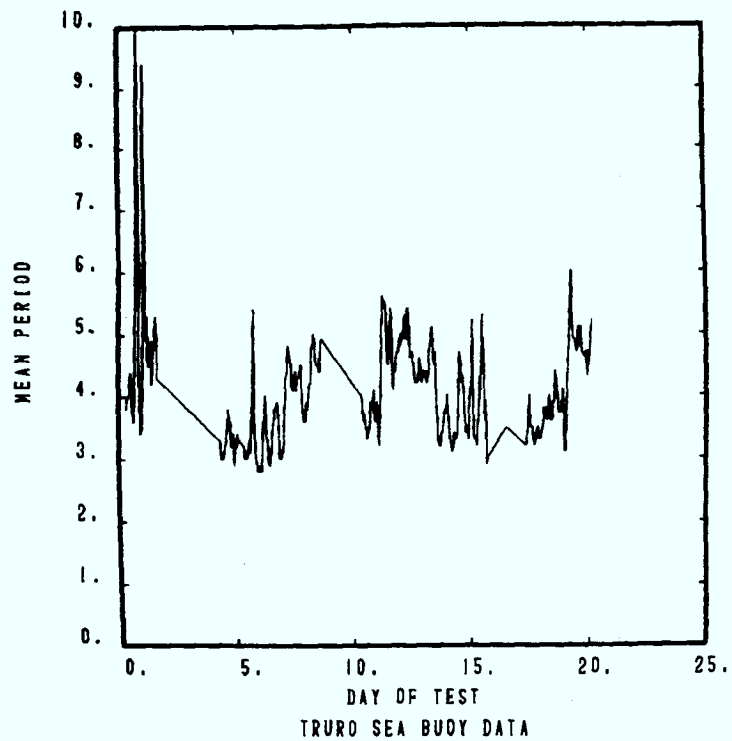


Figure A3 - Mean Period.

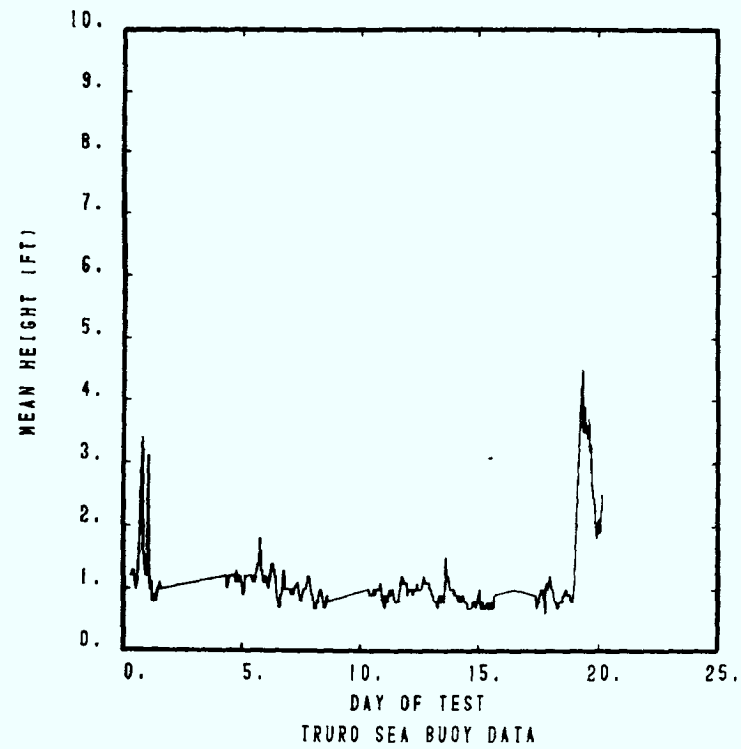


Figure A4 - Mean Height.

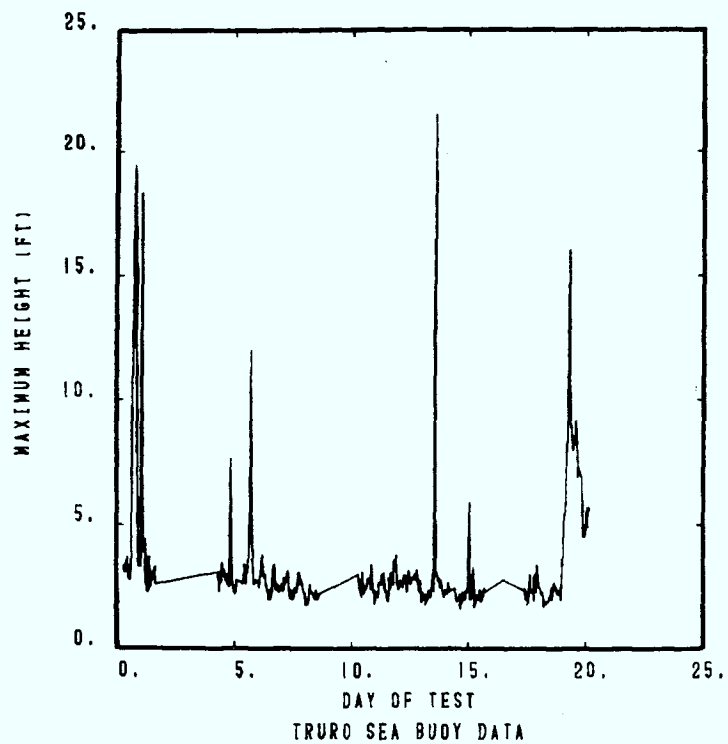


Figure A5 - Maximum Height.

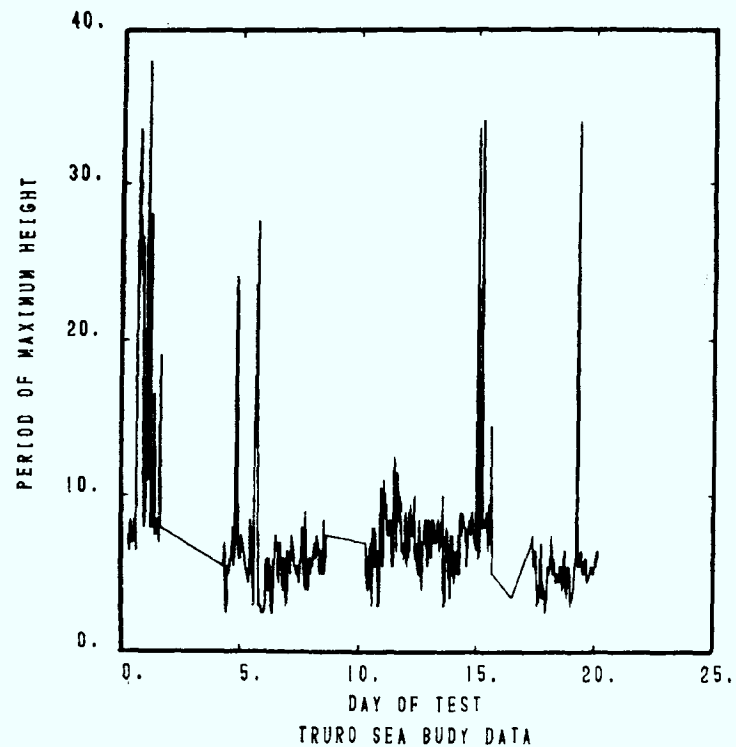


Figure A6 - Period of Maximum Height.

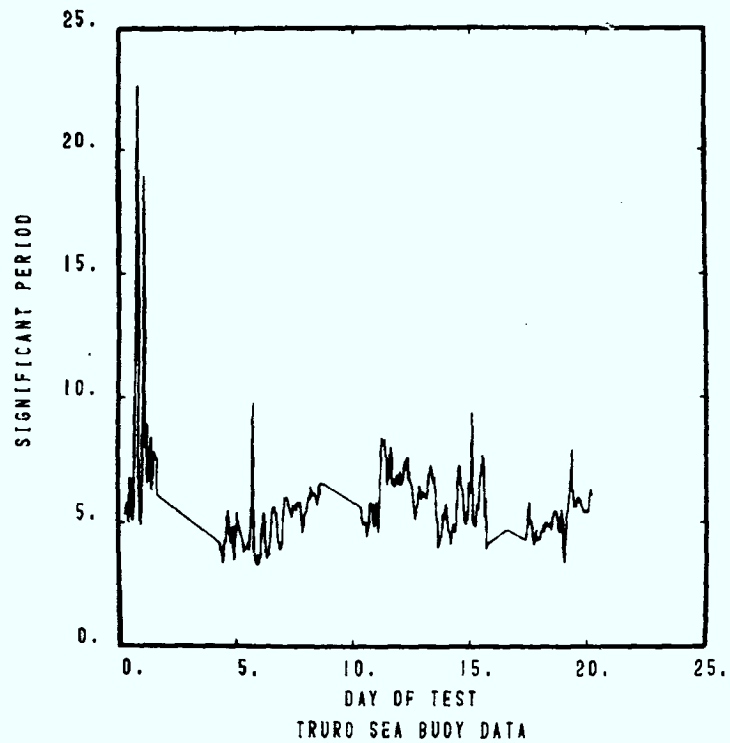


Figure A7 - Significant Period.

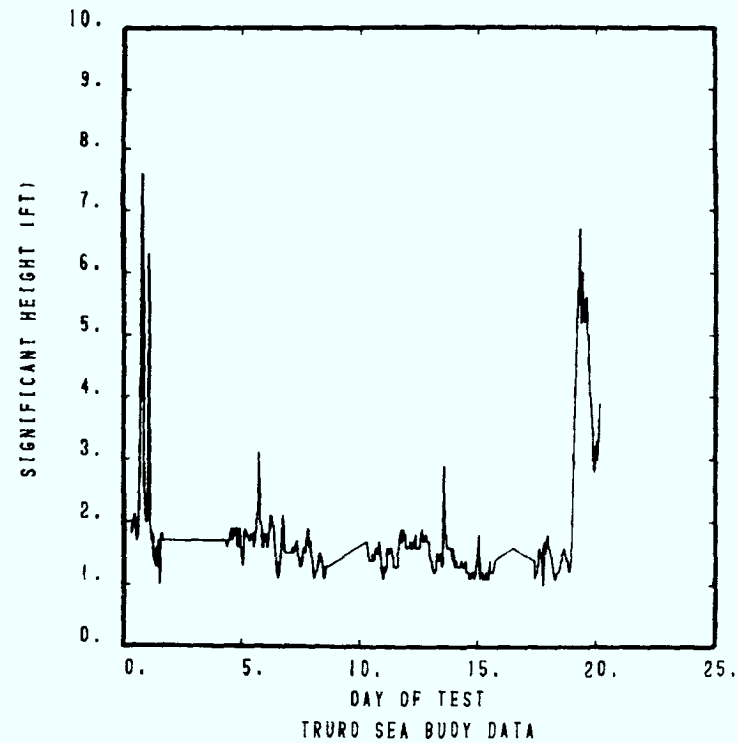


Figure A8 - Significant Height.

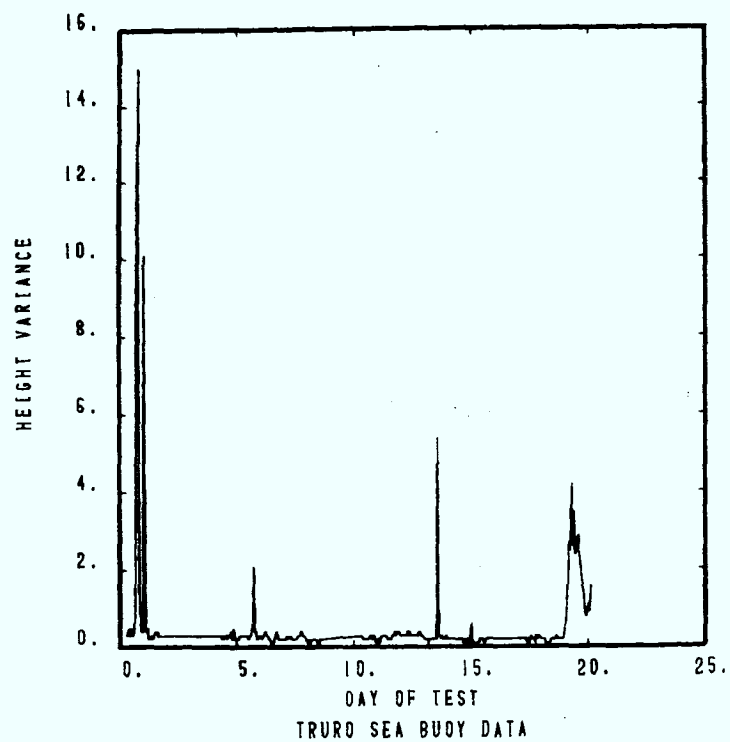


Figure A9 - Height Variance.

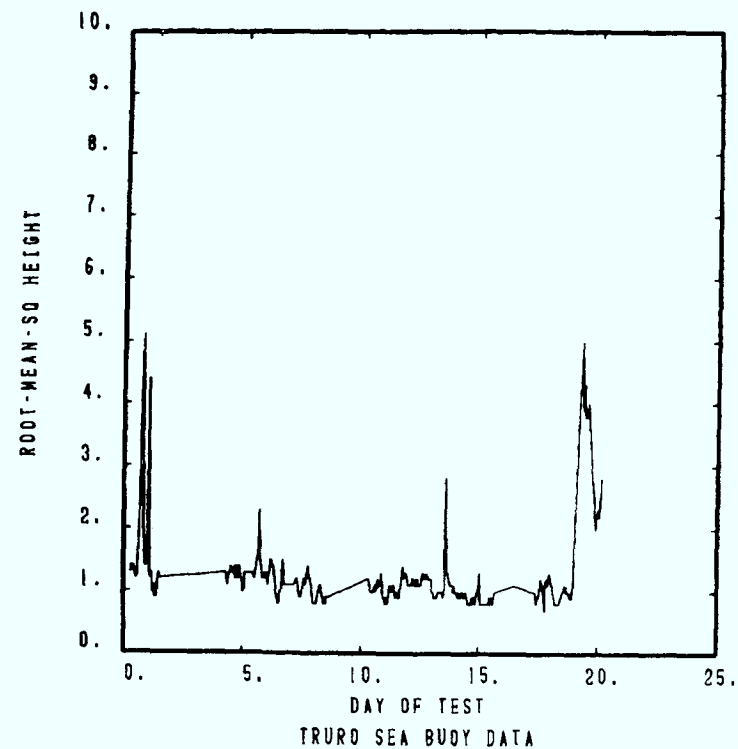


Figure A10 - R.M.S. Height.

$$\alpha \approx \frac{4}{\pi} (\text{sample mean})^2 \quad (\text{B1.5})$$

B.2 Weibull Processes

The probability density function for a Weibull random process is defined as:

$$p(x) = \frac{n}{\alpha} (x)^{n-1} \exp(-\frac{x^n}{\alpha}) \quad 0 \leq x \leq \infty \quad (\text{B2.1})$$

where parameters n and α are to be estimated from sampled data of this process.

The first moment is given by:

$$\langle x \rangle_W = \int_0^{\infty} n \frac{x^n}{\alpha} \exp(-\frac{x^n}{\alpha}) dx \quad (\text{B2.2})$$

$$\text{Letting } y = \frac{x^n}{\alpha} \text{ so that } dy = \frac{nx^{n-1}}{\alpha} dx \text{ and } x = (\alpha y)^{1/n} \quad (\text{B2.3})$$

Substituting Eqn(B2.3) into Eqn(B2.2) yields:

$$\langle x \rangle_W = \int_0^{\infty} \frac{ny\alpha \exp(-y)}{nx^{n-1}} dy \quad (\text{B2.4})$$

$$= \int_0^{\infty} \frac{1}{\alpha^{\frac{1}{n}}} \frac{1}{y^{\frac{1}{n}}} \exp(-y) dy$$

From table of definite integrals, we have:

$$\int_0^{\infty} y^n \exp(-ay) dy = \frac{\Gamma(n+1)}{a^{n+1}} \quad (\text{B2.5})$$

where $\Gamma(n)$ is the Gamma function.

Consequently,

$$\langle x \rangle_W = \frac{1}{\alpha^n} \int_0^\infty \frac{1}{y^n} \exp(-y) dy = \frac{1}{\alpha^n \Gamma(\frac{1}{n}+1)} \quad (\text{B2.6})$$

Since there are two unknown variables, α and n , another equation is needed for their solution. This equation can be obtained by considering the second moment. The second moment of a Weibull random process is defined as:

$$\langle x^2 \rangle_W = \int_0^\infty \frac{n x^{n+1}}{\alpha} \exp(-\frac{x^n}{\alpha}) dx \quad (\text{B2.7})$$

Using Eqn(B2.3), we have:

$$\langle x^2 \rangle_W = \alpha^{\frac{2}{n}} \int_0^\infty \frac{2}{y^{\frac{2}{n}}} \exp(-y) dy = \alpha^{\frac{2}{n}} \Gamma(\frac{2}{n}+1) \quad (\text{B2.8})$$

The first and second moments can be approximated from the sample mean and the sample variance, respectively. Squaring both sides of Eqn(B2.6) and taking the ratio between the result and Eqn(B2.8), we have:

$$\frac{\langle x \rangle_W^2}{\langle x^2 \rangle_W} = \frac{[\Gamma(\frac{1}{n}+1)]^2}{\Gamma(\frac{2}{n}+1)} \approx \frac{(\text{sample mean})^2}{(\text{sample 2nd moment})} \quad (\text{B2.9})$$

Eqn(B2.9) is a transcendental equation and can most easily be solved numerically. Using Newton's method, the location of the roots to the following equation will yield the value of n .

$$y = \langle x \rangle_W^2 \Gamma(\frac{2}{n}+1) - \langle x^2 \rangle_W [\Gamma(\frac{1}{n}+1)]^2 = 0 \quad (\text{B2.10})$$

The parameter α can then be found by substituting n into either Eqn(B2.6) or Eqn(B2.8).

B.3 Log-normal random processes

The probability density function for a log-normal random process is defined as:

$$p(x) = \frac{1}{x\sigma(2\pi)^{\frac{1}{2}}} \exp\left\{-\frac{(\ln x - m)^2}{2\sigma^2}\right\} \quad (\text{B3.1})$$

$$0 \leq x \leq \infty$$

where parameters m and σ are to be estimated from sampled data of this process.

The first moment of a log-normal process is defined as:

$$\langle x \rangle_L = \int_0^\infty \frac{1}{\sigma(2\pi)^{\frac{1}{2}}} \exp\left[-\frac{(\ln x - m)^2}{2\sigma^2}\right] dx \quad (\text{B3.2})$$

Using the transformation:

$$\begin{aligned} y &= \ln x & x &= \exp(y) \\ dy &= \frac{dx}{x} & dx &= \exp(y) dy \end{aligned} \quad (\text{B3.3})$$

we have:

$$\begin{aligned} \langle x \rangle_L &= \frac{1}{\sigma(2\pi)^{\frac{1}{2}}} \int_0^\infty \exp\left[-\frac{(y-m)^2}{2\sigma^2}\right] \exp(y) dy \\ &= \frac{1}{\sigma(2\pi)^{\frac{1}{2}}} \int_{-\infty}^\infty \exp\left[-\frac{y^2 - 2(m+\sigma^2)y + m^2}{2\sigma^2}\right] dy \end{aligned} \quad (\text{B3.4})$$

Let $z = (m + \sigma^2)$, and $z^2 = m^2 + 2m\sigma^2 + \sigma^4$.

It follows that $m^2 = z^2 - 2m\sigma^2 - \sigma^4$

$$\begin{aligned} \langle x \rangle_L &= \frac{1}{\sigma(2\pi)^{\frac{1}{2}}} \int_{-\infty}^\infty \exp\left\{-\frac{(y-z)^2}{2\sigma^2}\right\} \exp\left\{m + \frac{\sigma^2}{2}\right\} dy \\ &= \exp\left\{m + \frac{\sigma^2}{2}\right\} \end{aligned} \quad (\text{B3.5})$$

The second moment of a log-normal random process is defined as:

$$\langle x^2 \rangle_L = \int_0^\infty \frac{x}{\sigma(2\pi)^{\frac{1}{2}}} \exp\left[-\frac{(\ln x - m)^2}{2\sigma^2}\right] dx \quad (\text{B3.6})$$

Again using the transformation of Eqn(B3.3), we have:

$$\begin{aligned}\langle x^2 \rangle_L &= \int_{-\infty}^{\infty} \frac{1}{\sigma(2\pi)^{1/2}} \exp\left[-\frac{(y-m)^2}{2\sigma^2}\right] dy \\ &= \frac{1}{\sigma(2\pi)^{1/2}} \int_{-\infty}^{\infty} \exp\left\{-\frac{y^2 - 2(m+2\sigma^2)y + m^2}{2\sigma^2}\right\} dy\end{aligned}\quad (B3.7)$$

Letting $z = m + 2\sigma^2$, it follows that $z^2 = m^2 + 4m\sigma^2 + 4\sigma^2$. Consequently,

$$\begin{aligned}\langle x^2 \rangle_L &= \frac{1}{\sigma(2\pi)^{1/2}} \int_{-\infty}^{\infty} \exp[2(m+\sigma^2)] \exp\left[-\frac{(y-z)^2}{2\sigma^2}\right] dy \\ &= \exp[2(m+\sigma^2)]\end{aligned}\quad (B3.8)$$

The model parameters m and σ for a log-normal process are determined by first estimating the first and second moments from the sample mean and sample variance and then solving the following set of simultaneous equations:

$$\begin{aligned}\sigma^2 &= \frac{1}{2} \ln[\langle x^2 \rangle_L] - m \\ m &= \ln[\langle x \rangle_L] - \frac{\sigma^2}{2}\end{aligned}\quad (B3.9)$$

7. REFERENCES

- [1] M.W. Long, "Radar Reflectivity of Land and Sea", D.C. Heath and Company, Lexington Massachusetts, 1975.
- [2] M.I. Skolnik, "Radar Handbook", McGraw-Hill Book Company, New York, New York, 1970.
- [3] J.R. Conlon, "High Resolution radar, Part II - Sea-Clutter Measurements", Naval Res. Lab. Report NRL-4951, Washington, D.C., August 29, 1957.
- [4] J.C. Daley, "Sea-Clutter Measurements at X and C Band", Naval Res. Lab. Letter Report 5270-18A:JCD, August 23, 1966.
- [5] F.E. Nathanson, "Radar Design Principles", McGraw-Hill Book Company, New York, New York, 1969.
- [6] I.D. Olin, "Amplitude and Temporal Statistics of Sea Spike Clutter", International Conference Radar-82, pp.198-202.

- [7] M.M. Horst, F.B. Dyer and M.T. Tuley, "Radar Sea-Clutter Model", URSI Digest, 1978 International IEEE AP/S URSI Symposium, College Park, Maryland, U.S.A.
- [8] A.V. Oppenheim and R.W. Schaffer, "Digital Signal Processing", Prentice-Hall, Inc., Englewood Cliffs, New Jersey, 1975.
- [9] L.R. Rabiner and B. Gold, "Theory And Application Of Digital Signal Processing", Prentice-Hall, Inc., Englewood Cliffs, New Jersey, 1975.
- [10] J. Maaloe, "Sea-Clutter Statistics", International Conference Radar-82, pp. 193-202.
- [11] K.D. Ward, "A Radar Sea-Clutter Model and its Application to Performance Assessment", International Radar Conference Radar-82, pp.203-207.
- [12] A.M. Findlay, "Sea-clutter Measurement by Radar-return Sampling", Naval Research Laboratory Report 6661, February 12, 1968.
- [13] J.D. Delorenzo, E.S. Cassedy, "A Study of the Mechanism of Sea Surface Scattering", IEEE Transactions on Antenna and Propagation, Vol. AP-14, No.5, September 1966, pp.611-620.
- [14] G.V. Trunk and S.F. Geroge, "Detection of Target in Non-Gaussian Sea-Clutter", IEEE Transactions on Aerospace and Electronic Systems, Vol. AES-6, No.5, September 1970, pp.620-628.
- [15] C.I. Beard, "Behavior of Non-Rayleigh Statistics of Microwave Forward Scatter from a Random Water Surface", IEEE Transactions on Antennas and Propagation, Vol.AP-15, No.5, September 1967, pp.649-657.
- [16] A. Papoulis, "Probability, Random Variables, and Stochastic Processes", McGraw-Hill Book Company, New York, 1965.
- [17] F.B. Hildebrand, "Introduction To Numerical Analysis", McGraw-Hill Book Company, New York, N.Y., 1956.
- [18] I. Guttman. "Introductory Engineering Statistics", John Wiley and Sons, Inc., New York, New york, 1965.
- [19] M. Abramowitz and I.A. Stegun, Editors, "Hand Book Of Mathematical Functions", Dover Publications, Inc. New York, N.Y., 1965.

ACKNOWLEDGEMENTS

The author wishes to thank the personnel of Group 45 of the MIT Lincoln Laboratory for their cooperation in acquiring the sea-clutter data. Thanks are also due Mr. K.H. Wu for reviewing this report. This work was supported by the Department of National Defence, Ottawa, Canada under Research and Development Sub-program 33C89.

SECURITY CLASSIFICATION OF FORM
(highest classification of Title, Abstract, Keywords)

DOCUMENT CONTROL DATA

(Security classification of title, body of abstract and indexing annotation must be entered when the overall document is classified)

1. ORIGINATOR (the name and address of the organization preparing the document. Organizations for whom the document was prepared, e.g. Establishment sponsoring a contractor's report, or tasking agency, are entered in Section B.) Communications Research Centre 3701 Carling Avenue, P.O. Box 11490, Station H Ottawa, Ontario, K2H 8S2		2. SECURITY CLASSIFICATION (overall security classification of the document, including special warning terms if applicable) UNCLASSIFIED	
3. TITLE (the complete document title as indicated on the title page. Its classification should be indicated by the appropriate abbreviation (S,C,R or U) in parentheses after the title.) MULTI-FREQUENCY MEASUREMENT OF RADAR SEA CLUTTER AT LOW GRAZING ANGLES			
4. AUTHORS (Last name, first name, middle initial. If military, show rank, e.g. Doe, Maj. John E.) CHAN, H.C.			
5. DATE OF PUBLICATION (month and year of publication of document) May 1987	6a. NO. OF PAGES (total containing information. Include Annexes, Appendices, etc.) 65	6b. NO. OF REFS (total cited in document) 19	
7. DESCRIPTIVE NOTES (the category of the document, e.g. technical report, technical note or memorandum. If appropriate, enter the type of report, e.g. interim, progress, summary, annual or final. Give the inclusive dates when a specific reporting period is covered.) CRC Report No. 1410			
8. SPONSORING ACTIVITY (the name of the department project office or laboratory sponsoring the research and development. Include the address.) Defence Research Establishment Ottawa Department of National Defence Ottawa, Ontario, K1A 0Z4			
9a. PROJECT OR GRANT NO. (if appropriate, the applicable research and development project or grant number under which the document was written. Please specify whether project or grant) 041LC	9b. CONTRACT NO. (if appropriate, the applicable number under which the document was written)		
10a. ORIGINATOR'S DOCUMENT NUMBER (the official document number by which the document is identified by the originating activity. This number must be unique to this document.) CRC Report No. 1410	10b. OTHER DOCUMENT NOS. (Any other numbers which may be assigned this document either by the originator or by the sponsor)		
11. DOCUMENT AVAILABILITY (any limitations on further dissemination of the document, other than those imposed by security classification) <input checked="" type="checkbox"/> (x) Unlimited distribution <input type="checkbox"/> () Distribution limited to defence departments and defence contractors; further distribution only as approved <input type="checkbox"/> () Distribution limited to defence departments and Canadian defence contractors; further distribution only as approved <input type="checkbox"/> () Distribution limited to government departments and agencies; further distribution only as approved <input type="checkbox"/> () Distribution limited to defence departments; further distribution only as approved <input type="checkbox"/> () Other (please specify):			
12. DOCUMENT ANNOUNCEMENT (any limitation to the bibliographic announcement of this document. This will normally correspond to the Document Availability (11). However, where further distribution (beyond the audience specified in 11) is possible, a wider announcement audience may be selected.)			

UNCLASSIFIED

SECURITY CLASSIFICATION OF FORM

DCD03 9/04/87

13. ABSTRACT (a brief and factual summary of the document. It may also appear elsewhere in the body of the document itself. It is highly desirable that the abstract of classified documents be unclassified. Each paragraph of the abstract shall begin with an indication of the security classification of the information in the paragraph (unless the document itself is unclassified) represented as (S), (C), (R), or (U). It is not necessary to include here abstracts in both official languages unless the text is bilingual).

Sea-clutter has been and continues to be a major source of performance limitations for maritime surveillance radar systems. An understanding of the detailed sea-clutter behaviour is important in devising signal processing algorithms aimed at optimizing radar detection performance under sea-clutter environments.

A sea-clutter measurement experiment was conducted in July 1982 at North Truro (near Cape Cod), Massachusetts. The radar equipment employed was a multi-frequency, mobile coherent radar operated by Lincoln Laboratory of the Massachusetts Institute of Technology(MIT). Sea-clutter data were collected at X, S, L, UHF and VHF bands.

Because of interferences in the UHF and VHF bands, only X-, S- and L-band data are analyzed. Analyses have been carried out examining the sea-clutter coefficient as a function of frequency, polarization and waveform resolution. Spectral characteristics of sea-clutter in up-wind, cross-wind and down-wind conditions are compared.

14. KEYWORDS, DESCRIPTORS or IDENTIFIERS (technically meaningful terms or short phrases that characterize a document and could be helpful in cataloguing the document. They should be selected so that no security classification is required. Identifiers, such as equipment model designation, trade name, military project code name, geographic location may also be included. If possible, keywords should be selected from a published thesaurus, e.g. Thesaurus of Engineering and Scientific Terms (TEST) and that thesaurus identified. If it is not possible to select indexing terms which are Unclassified, the classification of each should be indicated as with the title.)

Sea-clutter

Radar

Measurement

--Multi-frequency measurement of radar sea clutter at low-grazing angles

TK
5102.5
C673e
#1410

[illegible]

201-6503

Printed
in USA

CRC LIBRARY/BIBLIOTHEQUE CRC
TK5102.5 C673e #1410 c. b

INDUSTRY CANADA / INDUSTRIE CANADA



209151

